Templated Colloidal Crystals with Collective Optical Properties

Master thesis by Nika Kutalia

Supervisors: Dr. Cyrille Hamon, Dr. Marianne Impéror-Clerc, PhD student Jules Marcone

SERP+ Erasmus Mundus Joint Master Program

MSc in Chemistry, Université Paris-Saclay | MSc in Nanomaterials Science and Technology, Universidade do Porto

August 2024

Table of contents

ACKNOWLEDGEMENTS: 3
LIST OF ABBREVIATIONS: 3
ABSTRACT: 4
1) INTRODUCTION: 5
1.1:Plasmonic properties of metal nanoparticles: 5
1.2: Controlling and designing the synthesis of colloidal anisotropic Au nanoparticles: 6
1.3:Evaporation-Induced Self-assembly (EISA) of anisotropic nanoparticles: 7
1.4:Template-assisted self-assembly of NPs in confinement and challenges in this field: 9
1.5: Hypotheses and perspectives: 11
2) EXPERIMENTAL METHODS: 12
2.1: Synthesis of Au nanoparticles: 12
2.2: Template-assisted self-assembly of metal nanoparticles: 14
2.3: Characterization techniques: 14
3) RESULTS AND DISCUSSION: 16
3.1: Size and shape-controlled synthesis of metal NPs: 16
3.2: Size analyses and optical properties of the synthesized NPs: 17
3.3: Templated EISA of nanoparticles in prismatic confinement: 21
CONCLUSION AND PERSPECTIVES: 28
REFERENCES: 29

ACKNOWLEDGEMENTS:

***I am very grateful and thankful**:*

To my supervisors Dr. Cyrille Hamon, Dr. Marianne Impéror-Clerc, and Jules Marcone for guiding me through the project and giving me very helpful pieces of advice and insights that helped me to write the thesis and conduct experiments.

To Jaime Gabriel C. Trazo, Rahul Nag, and Claire Hotton for being supportive and helping me to grasp new concepts as well as being good friends outside the lab.

To Claire Goldmann for teaching me how to synthesize gold nanoparticles and bringing positive energy into the lab.

To SERP+ program and EACEA that gave me the possibility to conduct research and allowed me to choose my future career.

To all the professors and teaching staff from my past till now who played an important role in helping me reach where I am now.

To my family members who were always supportive when I needed.

LIST OF ABBREVIATIONS:

1D	One dimensional
2D	Two dimensional
3D	Three dimensional
5-BrSA	5-Bromosalicylic acid
AA	Ascorbic Acid
AR	Aspect ratio
AuBP@Ag PRs	Gold core and silver shell pentagonal rods
Au BPs	Gold bipyramids
Au NRs	Gold nanorods
CMC	Critical Micelle Concentration
CTAB	Cetyltrimethylammonium bromide
CTAC	Cetyltrimethylammonium Chloride
EISA	Evaporation induced self-assembly
Fig.	Figure
LSPR	Localized surface plasmon resonance
NCs	Nanocubes
NDs	Nanodumbells
NPs	Nanoparticles
PDI	Polydispersity index
SAXS	Small-angle X-ray scattering
SCs	Supercrystals
SEM	Scanning electron microscope
SERS	Surface Enhanced Raman Scattering
TEM	Transmission electron microscope
UV-Vis-NIR	Ultraviolet-visible-near infra-red

ABSTRACT:

Inorganic nanoparticles (NPs) frequently self-assemble in nature in confinement, however tuning and controlling the assemblies is hard to achieve. Controlling the order of SCs and orientation of NPs can't be achieved by the drop-casting method (coffee-ring effect). Templated evaporation-induced self-assembly (EISA) in prismatic confinement is a promising method to create ordered SCs and tune the number of different oriented monodomains within prisms. Moreover, unlike spherical and cylindrical confinements, the confined geometry is not restricted to spherical and curved interfaces respectively. The formation of ordered SCs require careful design and control of size and shape of NPs, which are synthesized by seed mediated growth method and the size and shape of the synthesized NPs are assessed via UV-Vis-NIR spectroscopy and TEM technique. Two different NPs with different extents of anisotropy and tessellating effect were utilized for templated EISA in prismatic confinement. Small-angle X-ray scattering (SAXS) and scanning electron microscope (SEM) results showed the formation of tunable and ordered monodomains of AuBP@Ag 4 eq. PRs in prismatic confinement. For square and triangular prismatic molds, the formation of 4 and 3 monodomains respectively was observed. Moreover, SAXS demonstrated that PRs self-assemble in a 2D hexagonal phase. For the case of Au Tetrahedra, SEM images showed that Au Tetrahedra self-assemble into different structured SCs in prismatic confinement. In square prismatic shapes, the formation of a triangular phase was observed. For the case of triangular molds, the elements of dodecagonal quasicrystal (QC) and zig-zag-like structure and triangular phase were observed.

Keywords: Seed-mediated growth, plasmonic nanoparticles, self-assembly in confinement, colloidal SCs, small-angle X-ray scattering

Les nanoparticules (NPs) inorganiques s'assemblent fréquemment en confinement dans la nature, cependant, contrôler la formation et les propriétés de ces auto-assemblages peut s'avérer plus compliqué. Le contrôle de l'organisation des SCs et de l'orientation des NPs ne peut pas être obtenu par dépôt de goutte (effet tâche de café). L'auto-assemblage induit par évaporation (AAIE) en confinement dans des moules prismatiques est une méthode prometteuse pour obtenir des SCs organisés et sélectionner le nombre de monodomaines de différente orientation dans les prismes. De plus, contrairement à des moules sphériques ou cylindriques, la géométrie de confinement n'est pas restreinte à des interfaces incurvées. La formation de SCs ordonnés nécessite un grand contrôle de la taille et de la forme des NPs, qui sont synthétisées par recroissance de germes cristallins et leurs caractéristiques sont déterminées en spectroscopie UV-Vis-PIR et par MET. Deux types de NPs avec différentes anisotropies et symétries ont été utilisées pour l'AAIE en confinement dans des moules prismatiques. Les caractérisations en diffusion des rayons X aux petits angles (SAXS) et de la microscopie électronique par balayage (MEB) ont montré la formation de monodomaines ordonnées des PRs AuBP@Ag 4 eq. en confinement. Pour des moules prismatiques carrés ou triangulaires, la formation de respectivement 4 et 3 monodomaines a été observée. De plus, le SAXS a montré que les PRs s'assemblent en une phase hexagonale en 2D. Dans le cas des tétraèdres d'or, les images MEB ont montré qu'ils s'assemblaient autrement. Dans les moules prismatiques carrés, la formation d'une phase hexagonale a été observée. Dans le cas de moules trianglaires, des éléments de symétrie correspondant à des quasi-cristaux dodécagonaux ainsi qu'une structure en zig-zag et une structure hexagonale ont été observés.

Mots-clefs : Recroissance sur germes, nanoparticules plasmoniques, auto-assemblage en confinement, super-cristaux colloïdaux, diffusion rayons X aux petits angles

1) INTRODUCTION:

1.1:Plasmonic properties of metal nanoparticles:

Metal nanoparticles possess unique properties while interacting with electromagnetic waves. Upon the interaction of electromagnetic light with the metal nanoparticles, the conductive electrons are disturbed from their equilibrium positions.[1] The resulting collective oscillation of conductive electrons is known as localized surface plasmon resonance (LSPR).[1,2] Moreover, not all metals possess plasmonic frequencies in the visible region. LSPR frequencies are present in the UV region for most metals, while for alkali metals and some transition metals like Cu, Au, and Ag plasmon frequencies occur in the visible range.[2] LSPR is one class of surface plasmon resonance (SPR) in which collective oscillations are confined at the surface of NPs generating an electric field around them.[3] The dimension of interacting NP is lower than the incident wavelength, which is a requirement for LSPR.[3] In the second class of SPR which is denoted as surface plasmon polaritons (SPP), the charge oscillations couple with the incident light and propagate at the boundary between the metal and the dielectric medium strictly confining in 2D space.[3] Fig. 1 represents the two classes of SPR schematically:

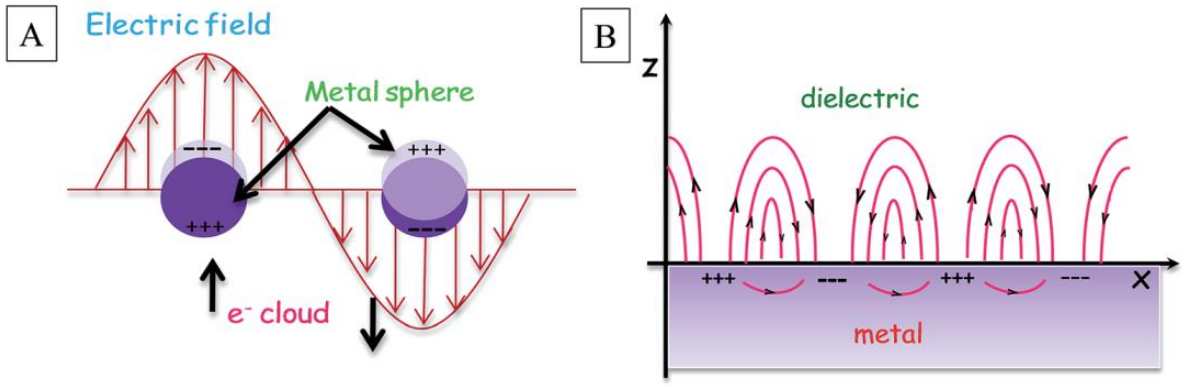
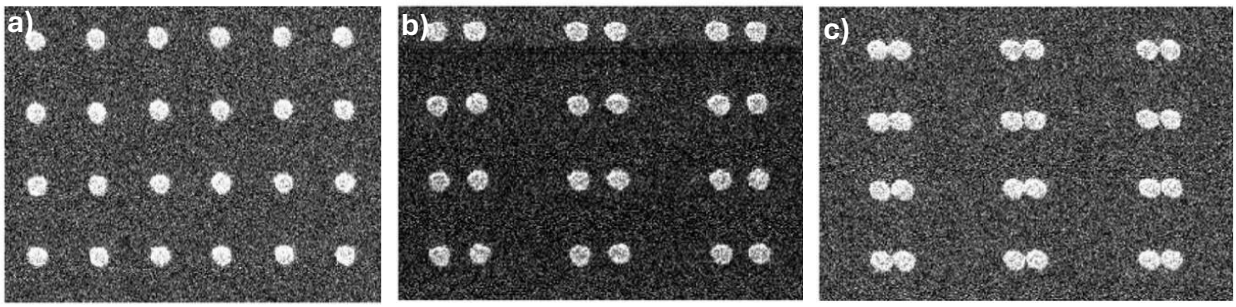


Fig. 1: Schematic representation of SPR phenomena: A) LSPR, B) SPP.[3]

Moreover, it is worth noting that surface plasmon resonance (SPR) is dependent on many factors: shape, size, surface morphology, and composition of NPs, as well as on the natural dielectric environment.[4] However, the most fascinating event happens when two plasmonic NPs interact with each other where the interaction can modify the optical properties of individual NPs.[5]



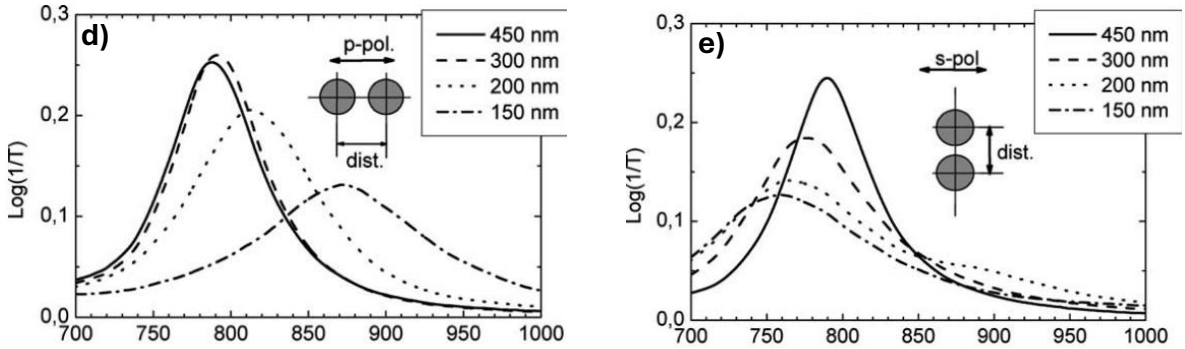


Fig. 2: SEM images of interacting Au NPs with different interparticle distances: a) 450 nm, b) 300 nm, c) 150 nm, and their extinction spectra where polarization direction of the light is parallel d) and perpendicular e) to long particle pair axis.[5]

Fig. 2a-c) represent SEM images of two interacting Au NPs with varying distances and Fig. 2d-e) their respective extinction spectra. It is evident that SPR peak changes, redshifts, or blueshifts depending on the polarization direction of the light concerning the long particle pair axis. When the polarization direction of the light is parallel to the long particle pair axis the change of SPR (red-shift) peak is significant with decreasing the interparticle distance.[5] Whereas, when the polarization direction of light is perpendicular to the long particle pair axis, the change in SPR (blue-shift) is smaller but easily observable.[5] Such coupling of plasmonic NPs generates hot spots (dramatic enhancement of the electric field between NPs) which make it possible to sense analytes at the molecular level with the technique called Surface Enhanced Raman Scattering (SERS).[6]

1.2: Controlling and designing the synthesis of colloidal anisotropic Au nanoparticles:

All systems try to decrease their total energy and become thermodynamically more favorable. Au NPs can adapt to various shapes which have different thermodynamic stability. They try to adopt spherical geometry because it has the least surface free energy for a given volume and is thus thermodynamically more favorable than other shapes.[7] Therefore, for the synthesis of anisotropic Au NPs, it is necessary to either break the symmetry of the spherical seeds by carefully controlling the reaction conditions or control its reaction kinetics which can be achieved by the seed-mediated growth method.[7] Moreover, with seed-mediated growth, it is possible to separate nucleation and growth from each other which makes it possible to control the size and shape of the synthesized NPs. For the case of Au NP synthesis, all the seed-mediated growth reactions require two major components: chloroauric acid ($HAuCl_4$) and stabilizing reagents such as cetyltrimethylammonium bromide or chloride (CTAB or CTAC). It was shown that cationic surfactants such as CTAB with CTA+ monomer electrostatically interact with anionic sites at the surface of Au NRs creating a bilayer around them.[8] However, the origin of the anionic sites of Au NRs is still not well understood since it is not well known whether the negative charge comes from bromide-related and silver-related species or other compounds.[8]

Except for the aforementioned two major components, a reducing agent such as ascorbic acid (AA) is required to reduce Au(III) into Au(I). The reduction is especially important since there is a comproportionation/disproportionation reaction between Au(III), Au(I), and Au(0): $Au^{3+} + 2Au^0 \leftrightarrow 3Au^+$ which is inclined towards the production of Au(I) (due to the stability of Au(I) species[9]), therefore Au(III) species can oxidize Au NPs or seeds. Also, it is important to use a weak reducing agent to make sure that the reduction of Au(III) species happens on the surface of the

seeds which act as catalysts and avoid second nucleation during the growth.[9] It is well-known that the crystallinity of the seeds governs the crystallinity of the synthesized NPs. For example: from single crystalline seeds one can synthesize Octahedra, octagonal rods, etc. from penta-twinned seeds bipyramids, and multiple twinned seeds can be used to synthesize pentagonal rods.[10] Fig. 4 schematically illustrates the importance of seeds' crystallinity and faults.

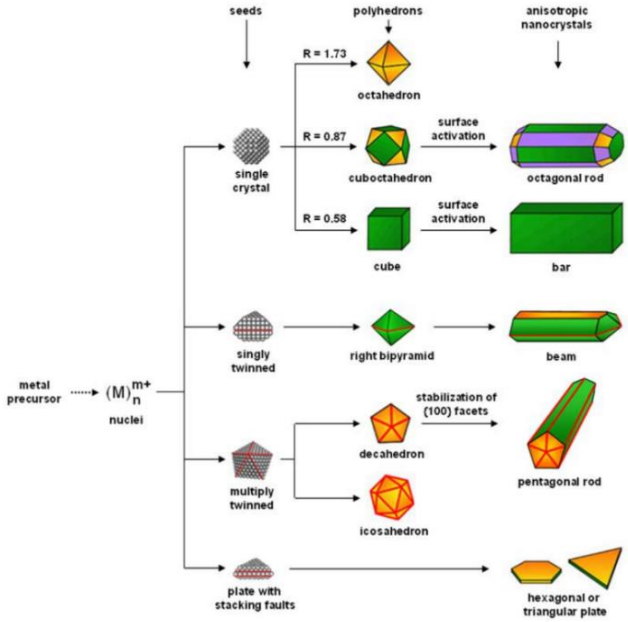


Fig. 3: Schematic illustration of the importance of the crystallinity and fault of the seeds for the synthesis of various-shaped nanoparticles.[7]

Finally, it is worth mentioning that the stabilization of certain crystal facets is important for controlling the equilibrium shapes of NPs. For example, halide ions (Cl^-, Br^-, I^-) and silver ions preferentially adsorb on certain crystal facets, stabilize them, and direct the growth of other facets, controlling the synthesized NPs' shape.[7] In particular iodide ions are adsorbed on {111} facets promoting the growth of 2D particles rather than oblong shapes.[7]

1.3:Evaporation-Induced Self-assembly (EISA) of anisotropic nanoparticles:

There are various assembly strategies to form ordered NP superstructures[11,12], however spontaneous self-assembly is a commonly used technique to prepare ordered structures of anisotropic NPs. One can distinguish two ways to spontaneously self-assemble anisotropic NP into superstructures[12]: solvent-evaporation and destabilization-based self-assembly (Fig. 4):

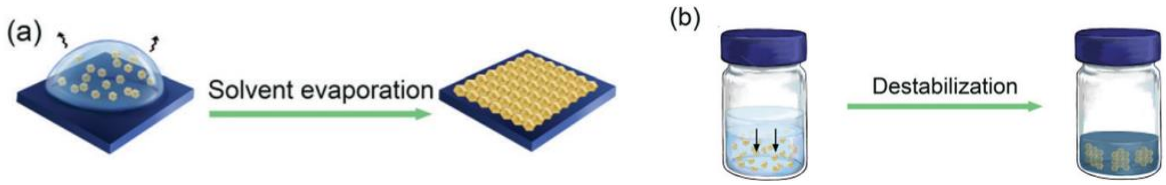


Fig. 4: Two ways to spontaneously self-assemble anisotropic NPs into SCs: a) solvent-driven evaporation-induced self-assembly, b) destabilization-driven self-assembly.[12]

In solvent-evaporation-driven self-assembly NPs deposit on a solid substrate and the solvent starts to evaporate at the solvent-air drying interface[12]. Initially, a disordered structure is formed which is eventually transformed into ordered structures as the concentration of the NPs increases[12]. It is interesting to note that the stabilizing agents such as CTAC and CTAB which initially stabilize NPs due to the presence of electrostatic forces, cause NPs to self-assemble when the volume of the solvent decreases since depletion forces become dominant[13]. One can conclude that when the volume of the solvent decreases NP dispersions interact with weak forces which enable them to form superstructures[12,13]. In destabilization-driven self-assembly, the non-solvent is added to the top of the solvent, and when the two phases mix, it causes NPs to destabilize and aggregate into superstructures. The reason behind it is the removal of stabilizing agents from NPs surfaces in the presence of a non-solvent which induces strong interactions between NPs.[12]

Droplet-evaporation-induced self-assembly causes Au nanorods (NRs) to self-assemble into various superstructures[14].

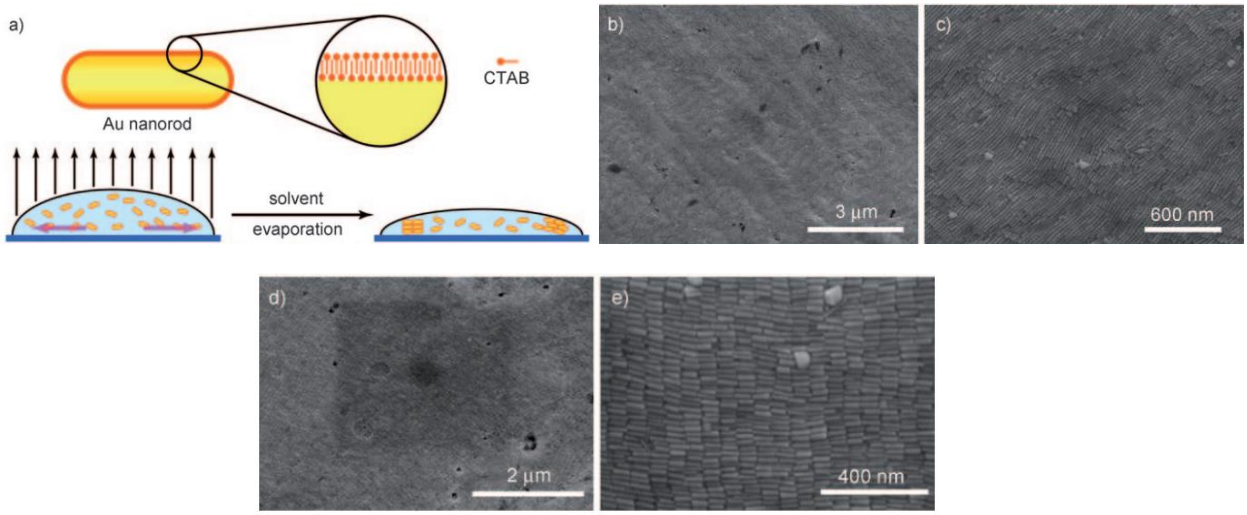


Fig. 5: Droplet-evaporation induced self-assembly of Au nanorods into ordered structures: a) schematic of the process, b) low-magnification image of a nematic phase, c) higher magnification image of the nematic phase, d) low-magnification image of a smectic phase, e) higher magnification image of the smectic phase.[14]

Fig. 5a) shows a scheme of droplet-evaporation-driven self-assembly of Au nanorods where the concentration of NPs at the edges of the droplet is higher than in the middle. After the solvent evaporates, the "coffee ring" is formed on the substrate into which the ordered structures can be found at the edges of the ring, whereas the middle area is relatively disordered.[11,14] Figs. 5c) and e) represent high-magnification SEM images of nematic and smectic phases formed by self-assembly of Au NRs. In the nematic phase, Au NRs assemble tip-by-tip manner where they create "wavy" structures, while in the smectic phase, Au NRs assemble side-by-side manner forming layers, but within the layers the orientation of Au NRs is random.[14] It is important to note that both in nematic and smectic phases Au NRs self-assemble mostly parallel to the substrate. Moreover, it must be pointed out that the concentration of stabilizing agents plays a major role in the formation of the ordered structures of Au NRs.[14] Only above the critical micellar concentration (CMC) of CTAB it is possible to have a bilayer on the surface of NPs which is necessary to avoid aggregation due to Van der Waals attractions leading to disordered structures.[14]

Anisotropic (direction-dependent) NPs such as Au NRs have predictable structures when the conditions are carefully controlled, and they do not possess many structural variations. However, one of the exceptions to this trend is Au Tetrahedra which possesses unique structural polymorphism depending on the conditions of self-assembly.[15,16] Wang et al. demonstrated that ligand length to edge length of tetrahedron ratio (softness) is a critical parameter to assess into which structure Au Tetrahedra self-assemble.[15] When there is a hard particle-like interaction (short ligand length/large tetrahedron edge), Au Tetrahedra self-assemble into a triangular phase.[15] When the softness increases Au Tetrahedra form a centered-rectangular structure and a further increase in softness makes it possible to form other structures which can be seen below:

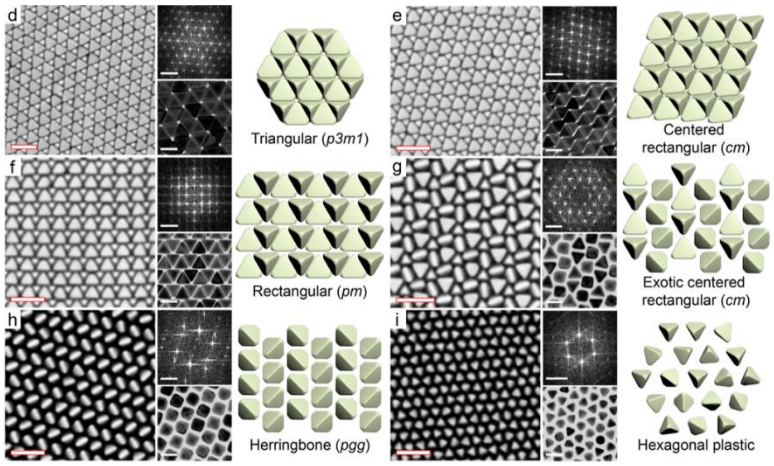


Fig. 6: Various structures into which Au Tetrahedra self-assembly by changing softness.[15]

Fig. 6 shows the various structures that Au Tetrahedra can adapt while self-assembling on a Si substrate in an evaporation-induced self-assembly process. Also, depending on CTAC concentration Au Tetrahedra self-assemble into different structures.[15] As Wang et al. demonstrated at low CTAC concentrations ($\leq$ 0.1 mM) the interactions between Au Tetrahedra are long-range repulsive, so the monoclinic phase is favored, whereas at high CTAC concentration ($\geq$ 2 mM) the depletion interactions are dominant favoring the hexagonal diamond phase.[15] Moreover, under very specific conditions Au Tetrahedra can self-assemble into dodecagonal quasicrystal.[16] Due to such structural variations of Au Tetrahedra, it is expected that the shape and size of the prismatic templates will affect the phase onto which Au Tetrahedra self-assemble. Therefore, unlike other anisotropic NPs (NRs, BPs) adapting the same structure for all shaped prismatic templates[17], for Au Tetrahedra the effective control of the formed structure in the templates is expected to be the case.

1.4:Template-assisted self-assembly of NPs in confinement and challenges in this field:

Tunning the structure and geometry of the self-assembly of Au NPs in confinement is challenging.[17] There have been many studies regarding the self-assembly of NPs in confinement. For example, Wang et al. investigated the self-assembly of NCs in emulsion droplets, however, the competition between the bulk and surface-induced structures caused the emergence of equilibrium defects making it hard to control confined geometry.[17,18] Wang et al. made Monte Carlo simulations of self-assembly of NCs in emulsion droplets by changing the parameter that they called asphericity α. For perfect spheres, the value of asphericity is 0 and it is 1 for sharp cubes.[18]

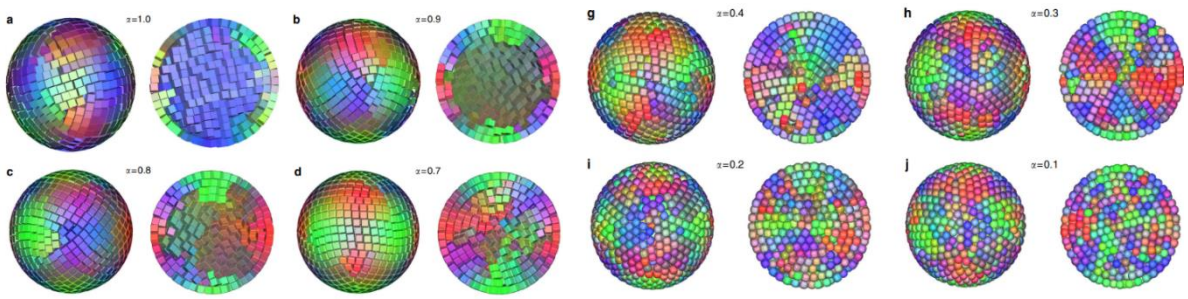


Fig. 7: Monte Carlo simulations of self-assembly of NCs in emulsion droplets by changing asphericity α.[18] (different colors are associated with different orientations)

As can be seen, they managed to get some ordered structures at the inner core of the sphere while modifying asphericity parameter. At α values of 0.4 and below the self-assembled structures seem to be disordered. Even though they managed to control orientational order to some extent, control of the confinement geometry was not achieved and the self-assemblies were limited to the spherical geometry.

Another study which investigated template-assisted self-assembly of nanodumbells (NDs) in confinement[19] showed interesting results which can be seen in Fig. 8:

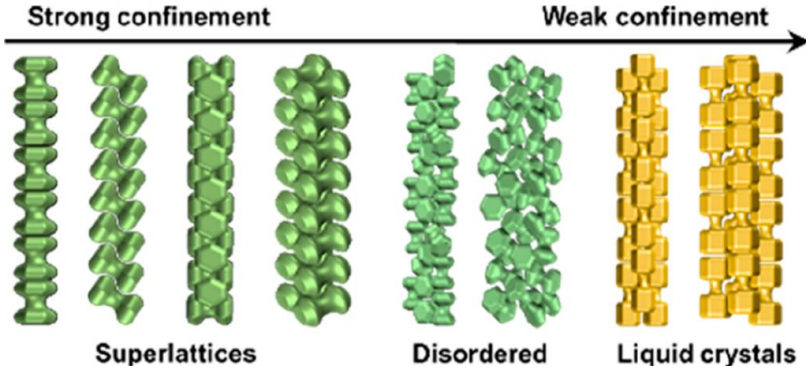


Fig. 8: Cylindrical template-assisted self-assembly of NDs in different confinement conditions.[19]

To produce such self-assembled structures, they dipped anodized aluminum oxide (AAO) cylindrical templates into NDs solution, and depending on the diameter of the AAO they were able to generate different structures. As can be seen, the structure into which NDs self-assemble depends on the confinement conditions. In strong confinement (small diameter), the self-assembly process is entropy-driven and as a result, the packing efficiency is maximized, favoring the formation of linear structures.[19] In weak confinement (large diameter), it is possible to form liquid crystals because the driving force is the maximization of packing efficiency. However, the formed superlattices are strictly restricted to a curved interface due to the cylindrical nature of the template.[17,19]

One method to generate different shaped and sized SCs and tune the number of differently oriented monodomains into which Au NRs self-assemble was investigated by Chaabani et al. from our group Matrix in Laboratoire de Physique de Solides (LPS)[17] and the master project is based on this study. By utilizing the templated EISA process, they self-assembled Au nanorods in prismatic confinement where they managed to control the number of monodomains (Fig. 9, showing 3 and 4 monodomains in triangular (A) and square (B) prismatic shapes respectively) while utilizing differently shaped prismatic templates. Unlike cylindrical confinement, the SCs were not restricted on the curved interface, and the number of oriented monodomains as well as the sizes of the SCs were carefully controlled.

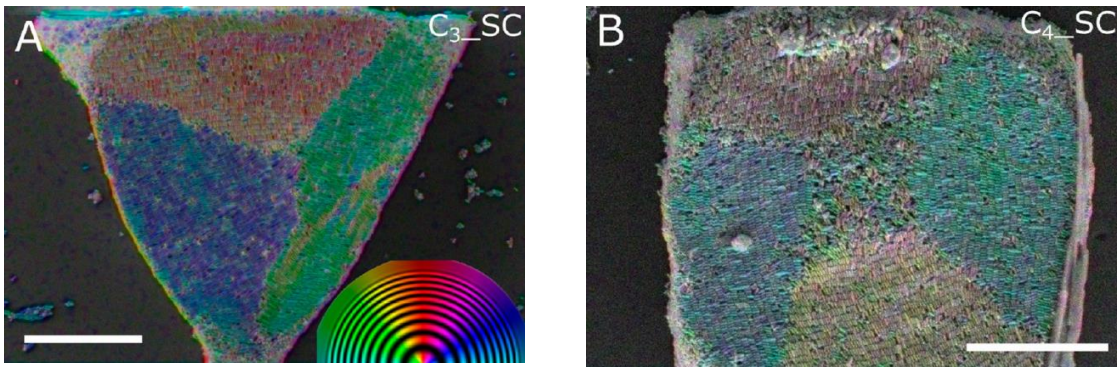


Fig. 9: Templated EISA of Au NRs in (A) triangular and (B) square prisms, showing 3 and 4 ordered and differently oriented monodomains.[17]

In this project template-assisted self-assembly of AuBP@Ag 4 eq. (PRs) was done to reproduce the results. However, Au Tetrahedra has never self-assembled in prismatic confinement and it is considered a novelty in this project. Chaabani et al.[17] have already demonstrated that for the case of Au NRs and Au BPs, the mold interface played a crucial role in governing the growth of monodomains (each mold interface governed the growth of one monodomain) until the monodomains encountered each other and grain boundaries formed between them.[17] Due to the interest in the results of this study, this master project aims to try templated EISA in prismatic confinement for more complex anisotropic NPs (AuBP@Ag 4 eq. (PRs), Au Tetrahedra) to see whether one can control the number of monodomains and the self-assembly structure of the SCs within the templates.

1.5: Hypotheses and perspectives:

After evaporation of a sessile droplet on a substrate, a coffee ring-like[11] structure is formed in which the edge has much more organized assemblies than the middle part of the sample and it is hard to control the orientation of the NPs.[14] With the templated EISA process due to the confinement effect, it is expected that the problem will be solved at least partially and more ordered and oriented structures will be formed within the sample.

AuBP@Ag 4 eq. (PRs), similarly to Au monocrystalline NRs do not fill a plane without any gaps (do not tile 2D plane). Therefore, they are expected to have a similar behavior as monocrystalline NRs while self-assembling in prismatic confinement. More specifically, one can expect a tunable number of monodomains depending on the selection of the shapes of templates. Therefore, for triangular and square prismatic molds, 3 and 4 monodomains are expected respectively. The second hypothesis is that the structure into which PRs self-assemble in the prismatic templates will

be similar to the structure into which Au NRs self-assemble. The third hypothesis is that due to the large size and aspect ratio (AR) and the shape of the tips (pentagonal vs octagonal for Au monocrystalline NRs), tip-by-tip interaction is expected to be even less likely which may affect the structure of the formed SCs (2D phase is more likely to be in case than 3D).

In the case of Au Tetrahedra, the situation is more challenging. As was already mentioned above, Au Tetrahedra tends to form many different phases due to the interplay between Van der Waals, depletion, and electrostatic forces.[20] Even though Au Tetrahedra do not tile the 3D space like Au NRs the extent of anisotropy is drastically different between the two. Consequently, different behavior is expected in prismatic confinement for Au Tetrahedra. Due to the short size of the CTAC ligand and the relatively large edge length of the Au Tetrahedron, it is expected that the interaction between Au Tetrahedra will be hard particle-like favoring the formation of a triangular phase. Moreover, due to the lesser extent of anisotropy (less directionality) than Au NRs it is less likely to have a formation of tunable oriented monodomains within the prismatic templates.

2) EXPERIMENTAL METHODS:

2.1: Synthesis of Au nanoparticles:

Synthesis of monocrystalline Au nanorods:

Seeds: 4.7 mL of 100 mM of CTAB solution was measured by a graduated cylinder and 50 µL of 25 mM of $HAuCl_4$ solution was added under fast stirring. 300 µL of 10 mM of $NaBH_4$ was added to the mixture under fast stirring. To avoid crystallization of the CTAB, a 30°C temperature was maintained throughout the synthesis.

Growth solution: 450 mg of 5-bromosalicylic acid (5-BrSA) (pre-reductant) was weighed into a 1 L Erlenmeyer flask to which 250 mL of a 100 mM CTAB solution and 240 mL of water were added. To dissolve 5-BrSA, sonication was performed. Finally, 476 µL of 100 mM of $AgNO_3$ along with 10 mL of 25 mM $HAuCl_4$ were added. UV-visible spectra of the mixture were taken until the peak absorbance reached 0.7 at 396 nm.

Preparation and purification of monocrystalline Au nanorods: 1250 µL of 100 mM of ascorbic acid and 800 µL of seeds solution were added to the growth solution. Firstly, a colorless solution was formed which is transformed into a brownish-reddish solution with time. After 4 hours at 30°C, the solution was centrifuged with 10000 rpm for 10 minutes, washed with water and redispersed in 2.5 mM of CTAC. The color of the formed sediment is brownish-red.

Synthesis of monocrystalline Au spheres:

Seeds: 9.4 mL of a 100 mM of CTAB solution was taken and 100 µL of a 25 mM $HAuCl_4$ solution was added. To which 10 mM of $NaBH_4$ solution was added. The formation of a brownish solution was observed.

Preparation of growth solution: 160 mL of 100 mM of CTAC solution was poured in a 250 mL Erlenmeyer flask. For the formed mixture, 3.2 mL of 25 mM of $HAuCl_4$ solution was added. Finally, 60 mL of 100 mM of AA solution was added to the mixture.

Preparation and purification of monocrystalline Au spheres: Finally, 8 mL of the seed solution was added to the growth solution and stirred for 1 hour at room temperature. Directly, the color of

the solution became wine red which indicates the formation of monodispersed gold spheres. After 1 hour, the synthesized monodispersed Au spheres were formed and divided into 8 tubes by centrifugation by SORVALL RC 5C centrifuge for 2 hours at a speed of 14 000 rpm. Such speed is necessary due to the small size of the spherical nanoparticles. Then, the nanoparticles were combined into 1 tube and the supernatant was disposed of. The spherical nanoparticles were prepared for the next centrifugation.

Synthesis of Au Bipyramids:

Preparation of pentatwinned seeds: 99 mL of DI water at 30°C was taken to which 7.94 mL of 756 mM CTAC solution was added. 1200 µL of 25 mM $HAuCl_4$ and 12 mL of 50 mM Na_3Cit were added to the mixture. After 30 min, under fast stirring 1 mL of 25 mM of $NaBH_4$ solution was added. The brownish colored solution was formed indicating the formation of low-sized NPs. UV-vis spectroscopy (Cary 5000) was taken to observe the initial TSPR peak appearance around 20 nm.

Growth solution: 200 µL of 100 mM of $AgNO_3$ solution was added to 200 mL of 100 mM of CTAB solution at 30°C under stirring. 4 mL of 25 mM of $HAuCl_4$ and 4 mL of 1 M of HCl were added to the resulting mixture. Finally, 1600 µL of ascorbic acid was added to the mixture.

Preparation and purification of Au bipyramids: When the solution became colorless after the addition of ascorbic acid, the appropriate amount of the seeds was added and was stirred at 30 °C for 4 hours. A series of centrifugations with the speed of 3000-3500 rpm for 30 minutes were performed for the purification of the solution. Finally, the appropriate amount of 450 mM of BDAC was added to the purified solution for depletion. After the addition of BDAC, the solution was left overnight for 16 hours.

Synthesis of Au Tetrahedra:

Seeds: For the synthesis of Au Tetrahedra, monocrystalline Au spheres were used as seeds.

Preparation and purification of Au Tetrahedra: In a round-bottom flask 24.94 mL of water was added at 30°C to which 2.54 mL of 756 mM of CTAC was added. In order to have the mixture of CTAC and CTAB, 480 µL of 1M of KBr was added. Then, 4 mL of 100 mM of AA was added. The amount of Au spheres to be added was $3.876*10^{-7}$ moles which was converted to the appropriate volume. Finally, with a syringe pump with a speed of 0.5 mL/hour 10 mL of 2.5 mM of $HAuCl_4$ was added, it is important for kinetic reasons to make sure that Tetrahedra are formed. After 20 hours the bluish solution was formed. After that series of centrifugations were performed for purification of the solution: 1st centrifugation 25 mins with the speed of 8000 rpm, followed by the 2nd centrifugation with the speed of 7500 rpm for 25 mins. Finally, for the depletion of Au Tetrahedra, the appropriate amount of 756 mM of CTAC was added. The formation of a pinkish solution after the addition of 756 mM of CTAC indicates the presence of spheres in the solution, whereas Au Tetrahedra sediment at the bottom.

Synthesis of Au Octahedra:

Seeds: For the synthesis of Au Octahedra, monocrystalline Au nanorods were used as seeds.

Growth solution: 20 mL of 10 mM of CTAB was put at 60°C to which 400 µL of 25 mM $HAuCl_4$ was added. Finally, 89 µL of butanoic acid was added to the resulting mixture after which the solution should become colorless.

Purification of Au Octahedra: The appropriate amount of monocrystalline Au nanorods seeds (depending on the R-value) were added to the growth solution and the solution was kept for 16 hours at 60 °C. The resulting solution was centrifuged at least twice at 5000-5500 rpm speed for 10 minutes.

2.2: Template-assisted self-assembly of metal nanoparticles:

Cleaning of silicon wafer and glass coverslips before self-assembly:

Both silicon wafers and glass coverslips were sonicated in ethanol for 5-10 minutes. After which the cleaning of their surface was performed by using O_3/UV cleaner for 45-60 minutes. The cleaning is necessary to make their surfaces more hydrophilic and remove impurities.

Preparation of a PDMS mold*:*

Sylgard 184 elastomer and curing agent with the ratio of 10:1 (by mass for preparation of relatively soft molds) was mixed carefully.[21] The resulting mixture was centrifuged at 2500 rpm speed for 2 minutes to remove the bubbles. The mixture was poured onto the Si master purchased from Blackhole lab and put in a vacuum oven at 70°C for 3 hours.

Template-assisted self-assembly:

Onto the prepared PDMS mold, 10 µL of concentrated NPs suspensions were dropped onto which silicon wafer (for SEM) and glass coverslip (for SAXS) substrates were placed. The self-assembly experiments were performed in a petri dish without humidity conditions. The approximate drying time was 16 hours after which the substrate was carefully removed.

2.3: Characterization techniques:

Optical microscopy:

The observation of a template-assisted self-assembly of metal NPs was performed by WITec Alpha300 Access optical microscope. Observation of the samples is based on the reflection of the light and an optical microscope is a powerful technique to assess the shape and size of the filled templates. Moreover, the technique was employed for determining the best positions for SAXS measurements and the initial assessment of the best concentration combinations of Au(0)/CTAC for the best possible template-assisted self-assembly of metal NPs. Optical microscope observations were done before SEM and SAXS characterizations for the initial assessment of the formed SCs.

UV-Visible-NIR-spectroscopy:

The measurement of extinction spectra of metal nanoparticles was performed by using a Cary 5000 dual-beam spectrophotometer. Approximately 2 mL of the metal NPs solutions in polystyrene cuvettes with 1 cm of path length were placed in the spectrophotometer and their extinction spectra in the range of 300-1400 nm wavelength were taken at room temperature. Via the spectrophotometer, the main plasmonic resonance bands of metal NPs, the presence of impurities in NPs solutions, as well as the extent of aggregation of NPs were found. Moreover, for Au NPs the concentration of Au(0) was approximated by noting the fact that at 400 nm for 1.2 absorbance the concentration of Au(0) is 0.5 mM.[9]

Transmission electron microscopy (TEM):

The images were acquired by utilizing of high-performance JEOL JEM-1400 TEM microscope with an accelerating voltage of 120 kV. By using TEM the images of Au NRs, BPs, Tetrahedra, Octahedra, and spheres were collected. Based on the images, the size distributions of the metal NPs were determined by using Image J software. Moreover, the information about polydispersity of NPs and the presence of impurities was found.

Scanning electron microscopy (SEM):

The images were acquired by using a Zeiss SUPRA55VP machine under the acceleration voltage of 5 kV and the value of the voltage for Everhart-Thornley-detector (EHT) based on secondary electrons was chosen to be 2-3 kV. By using SEM the structure and presence of monodomains (for AuBP@Ag 4 eq. PRs) as well as different structures for Au Tetrahedra have been found. Moreover, SEM made it possible to characterize 2D structures at the top of the crystals for metal NPs.

Small-angle X-ray scattering (SAXS):

SAXS and SANS are commonly employed characterization techniques to assess the organization of materials from angstrom to micrometer scale.[22,23] Moreover, SAXS can be effectively utilized to study the structure of any materials ranging from biomolecules and polymers to liquid crystals and glasses as well as for probing the structure of colloidal suspensions.[22] The idea behind the SAXS technique is to measure the scattering intensity (I) of X-rays vs its scattering angle.[22] Also, scattering intensity I is a function of q or scattering vector which is denoted by: $q = 4\pi\sin(\theta/\lambda)$, where 2θ, and λ are scattering angle and X-ray wavelength respectively.[22]

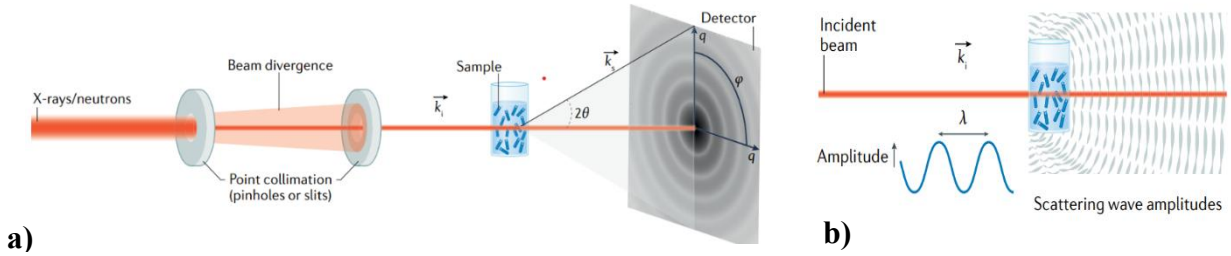


Fig. 10: Experimental set-up of SAXS a), scattered convolution b).[22]

It is apparent from Fig. 10a that the experimental set-up for SAXS consists of the source of X-rays and the optical devices defining the beam energy, shape, and direction.[22] The selected beams then are directed toward the sample where they are scattered with a scattering angle of 2θ and the scattered beam was recorded on the 2D detector placed after the sample. A scattered vector can also be defined as: $\vec{q} = \overrightarrow{k_s} - \overrightarrow{k_\iota}$, where $\overrightarrow{k_s}$ and $\overrightarrow{k_\iota}$ are scattered and incident wavevectors respectively. Fig. 10b shows the interaction of X-ray beams with the sample in the case where there is no change in λ (elastic scattering), and there is a constant distance between waves.[22] In that case, there is an occurrence of destructive and constructive interferences of the waves which are recorded on the 2D detector.

In this project, to get information regarding the crystal structure of metal NPs and the presence of the monodomains in the templates, as well as assessing the order of the formed SCs, full beam (size of $300 \times 300\ \mu m^2$) SAXS instrument with the rotating anode of Cu SAXS ($K_\alpha = 1.542$ Å)

detector of Eiger 4 M (Dectris Ltd, Switzerland) and sample to detector distance of 1.396 m at Laboratoire de Physique des Solides (LPS) was utilized.

3) RESULTS AND DISCUSSION:

3.1: Size and shape-controlled synthesis of metal NPs:

Various Au NPs (spheres, NRs, Octahedra, Tetrahedra, BPs) as well AuBP@Ag 4 eq. (PRs) were synthesized in this project. Fig. 11 below represents a scheme of the synthesis route of various NPs:

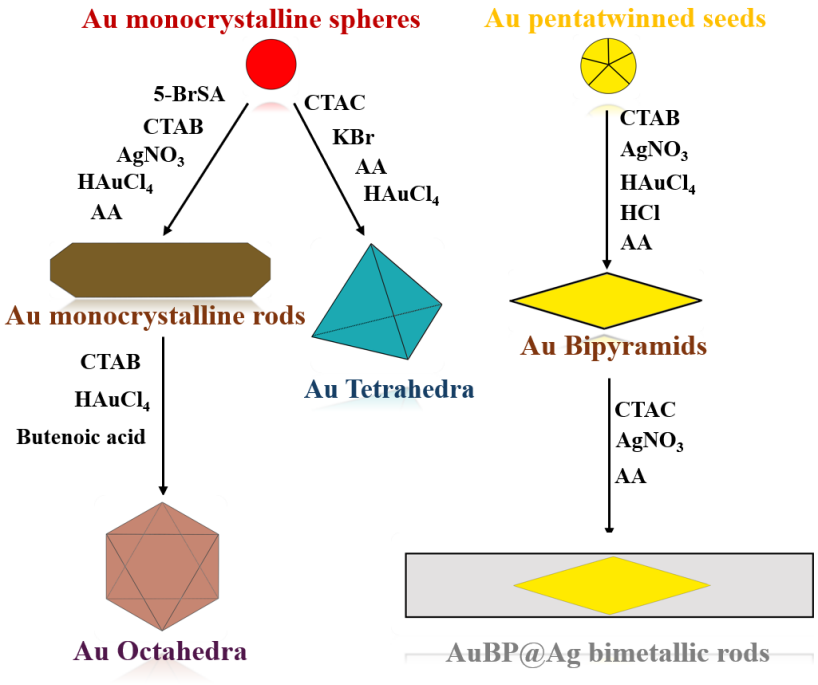


Fig. 11: A schematic representation of the synthetic route of the synthesized NPs.

It is important to note that for the syntheses of the NPs, seed-mediated growth[7,10] method was utilized. Along with the seeds, a growth solution containing of $HAuCl_4$, stabilizing agents such as CTAC and CTAB, shape-directing agents such as KBr or $AgNO_3$, and reducing agents (AA, butenoic acid, 5-BrSA) were employed. However, there is one more requirement to effectively synthesize the above-mentioned NPs. The nature and crystallinity of the seeds govern the symmetry and crystallinity of the synthesized NPs.[7,10] For example, since Au Octahedra and Au Tetrahedra are single-crystalline NPs,[10] it is necessary to utilize monocrystalline spheres as seeds. The same is true for Au Bipyramids which possess 5-fold symmetry and require pentatwinned seeds to be synthesized. On the other hand, the synthesis of pentatwinned seeds requires thermal treatment[24] for 5 days to ensure the effective twinning for the synthesis of pentatwinned NPs (BPs, AuBP@Ag PRs). However, for some NPs the additional requirement, the manipulation of the reaction kinetics is required. For instance, the dropwise addition of the growth solution[10,25] is necessary for the synthesis of Au Tetrahedra, since Au Tetrahedra are not thermodynamically stable products. The last important point that must be pointed out is related to the choice of the stabilizing,

shape-directing and reducing agents for the synthesis of the NPs which appear to be different for diverse NPs.

Au NRs require CTAB as a stabilizing agent because CTAB appears to form rod-like micelles directing an anisotropic growth and the presence of bromide ion is necessary for breaking symmetry.[9] It appears that with other surfactants such as CTAC and BDAC[9] the synthesis of monocrystalline rods can't be achieved. Moreover, the role of the Ag^{+} ions is still under debate, but it plays an important role in favoring the synthesis of monocrystalline rods over pentatwinned rods.[9] Moreover, 5-BrSA, a weak pre-reductant is necessary to tune the shape and optical response of Au NRs.[26]

For the case of Au Octahedra, the mild-reducing agent, butenoic acid is necessary to control the thermodynamics[27] of the reaction and have an effective synthesis of the NPs. Meanwhile, the dropwise addition[25] of the growth solution, as well as the mixture of CTAC and KBr play an important role in controlling the reaction kinetics for the synthesis of Au Tetrahedra as well as breaking the symmetry and favoring the anisotropic growth.

The reagents required for the synthesis of Au BPs are the same as the reagents necessary for the synthesis of Au NRs, but there is one important exception. The synthesis of Au BPs requires a careful control of the reducing power of AA whose reducing strength is quite sensitive to pH.[10] By adding HCl the reducing power of AA decreases which favors the formation of Au BPs.

The synthesis of AuBP@Ag 4 eq. (PRs) requires the deposition of Ag atoms on the surface of Au BP. In the case of 4 eq. PRs, the quantity of Ag(0) atoms compared to Au(0) atoms (from the BP seeds) were four times more.

3.2: Size analyses and optical properties of the synthesized NPs:

In this section, the size (dimensions) and optical properties of the synthesized NPs are assessed. The size analyses were performed by using ImageJ software while analyzing TEM images of NPs, and the optical response of NPs was assessed from UV-Visible-NIR spectra.

Au monocrystalline nanorods (NRs):

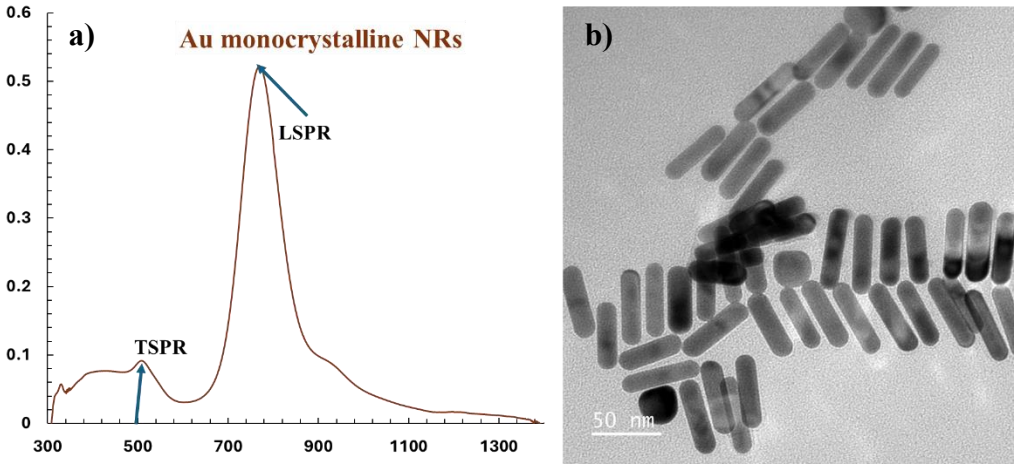


Fig. 12: a) UV-visible spectrum and b) TEM image of the synthesized Au NRs.

Synthesized Au NRs have two major bands at 771 nm and 507 nm corresponding to LSPR and TSPR modes respectively (Fig. 12a). The presence of a shoulder close to the TSPR band as well

as the ratio of absorbance of the LSPR band to the absorbance of TSPR band can be employed to assess the purity of the synthesized Au NRs.[9] The high ratio of the absorbances ($\frac{A_{LSPR}}{A_{TSPR}} = 5.69$) and insignificant contribution of the shoulder compared to the major bands indicate the purity of the synthesized Au NRs. The shoulder next to the LSPR band can be explained by the aggregation of Au NRs happening after the concentrating of Au NRs solution. Fig. 12b represents a TEM image of Au NRs from which the length and the diameter can be determined. The calculated length and diameter of the Au NRs along with their uncertainties can be seen in Table 1.

Table 1: Calculated dimensions along with their uncertainties of Au NRs:

	Au monocrystalline nanorods (NRs)
Length with uncertainty (nm)	51.555 ± 5.081
*PDI of length (%)	9.85
Diameter with uncertainty (nm)	13.335 ± 1.54
PDI of diameter (%)	11.5
Aspect ratio (AR)	3.87

PDI: Polydispersity index

The calculated data suggests that Au NRs are relatively monodispersed (especially concerning their length) suggesting the success of the employed synthesis method.

Au bipyramids (BPs):

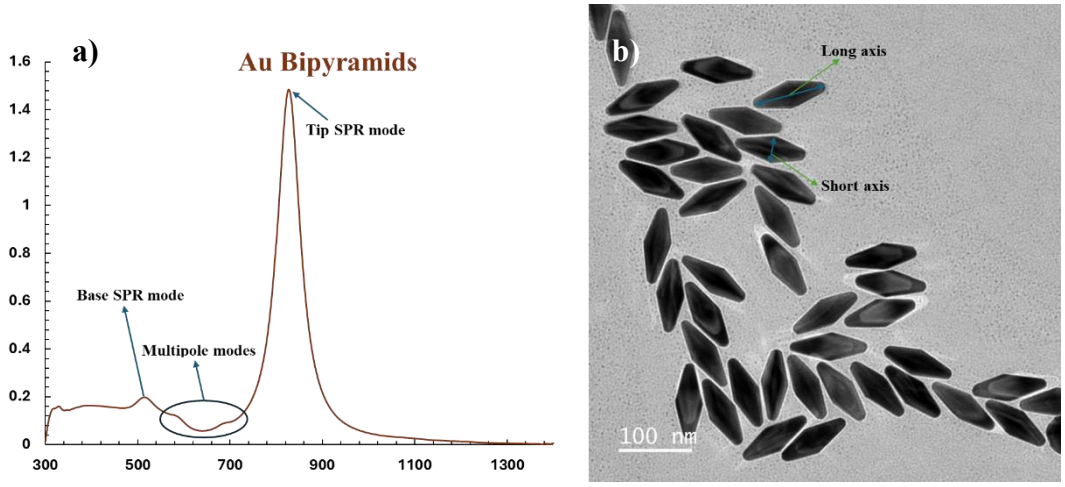


Fig. 13: a) UV-visible spectrum and b) TEM image of Au BPs.

Fig. 13 represents the UV-visible spectrum and TEM image of the synthesized Au BPs. From the UV-visible spectrum, it is apparent that there are two major bands at 827 nm and 510 nm corresponding to tip SPR and base SPR of Au BPs respectively.[28] Moreover, the appearance of multipole modes between tip SPR and base SPR modes is associated with the large size of the synthesized Au BPs.

Table 2: Calculated dimensions along with their uncertainties of Au BPs:

	Au monocrystalline nanorods (NRs)
Long axis with uncertainty (nm)	99.786 ± 2.76
PDI of long axis (%)	2.77
Short axis with uncertainty (nm)	36.592 ± 2.145
PDI of short axis (%)	5.86

Polydispersity of Au BPs is even lower than Au NRs which implies the good quality of the seeds and the success of the seed-mediated growth method.

Au Tetrahedra and Octahedra:

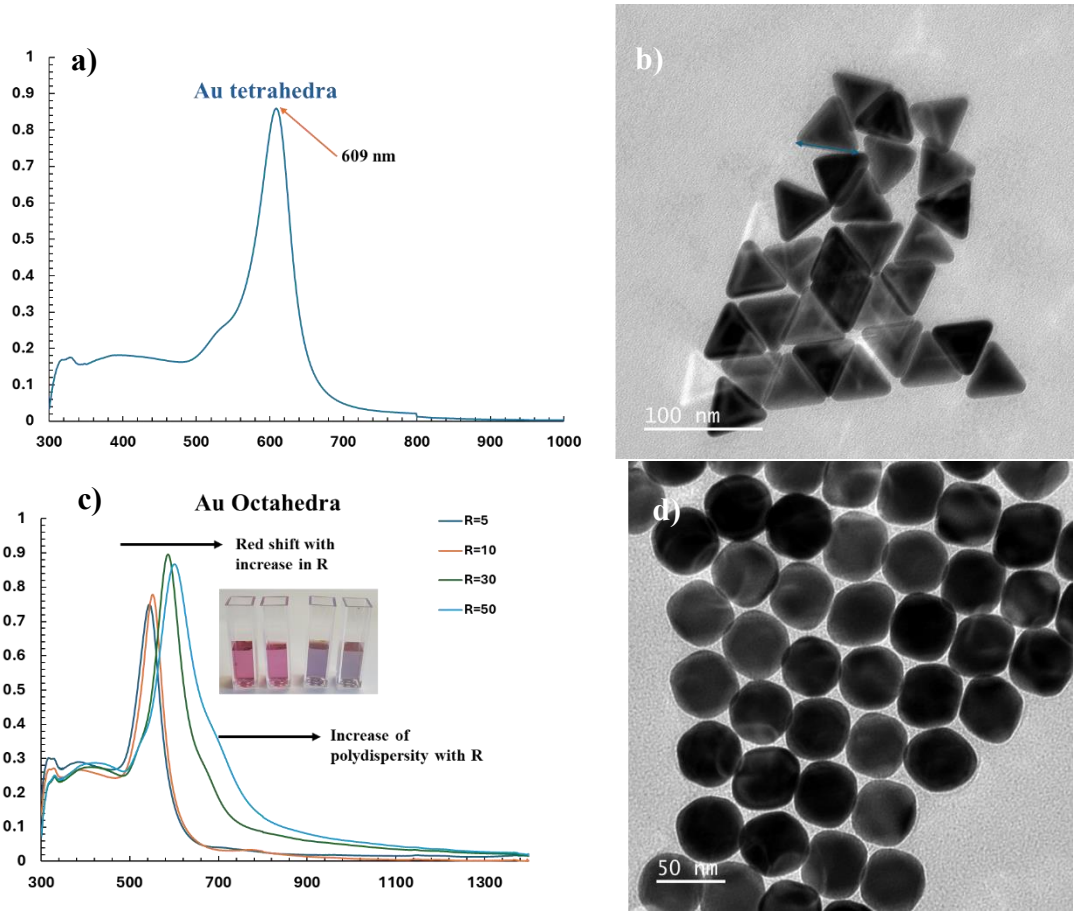


Fig. 14: a) UV-Visible spectrum and b) TEM image of Au Tetrahedra, c) UV-Visible spectra (R = 5, 10, 30, 50) and d) TEM image (R = 5) of Au Octahedra.

The major plasmonic peak of Au Tetrahedra is at 609 nm, whereas the band around 525 nm can be explained by two reasons. The first reason is the presence of some impurities (spheres, etc.) which is unavoidable even after purification of Au Tetrahedra. The other reason is that due to the relatively large size of the Au Tetrahedra, the hybridization of the quadrupole and dipole plasmonic vertex modes happens which is responsible for the appearance of this peak.[15]

4 different-sized Au Octahedra were synthesized in this project from Au monocrystalline nanorods. Via the synthesis method described in the experimental section, it was possible to tune

the size of Au Octahedra by varying the value of the molar ratio of $HAuCl_4$ to Au NRs seed, R. From Fig. 14c, it is possible to observe that when the value of R increases the major plasmonic band red-shifts and the polydispersity increases. Furthermore, the color of the solution becomes more bluish. The results fully agree with the previously conducted study dealing with the syntheses and self-assembly of different-sized Au Octahedra.[27]

Table 3: Calculated dimensions of Au Tetrahedra and Octahedra (R = 5):

	Au Tetrahedra	Au Octahedra (R = 5)
Edge length (nm)	44.285 ± 2.417	39.087 ± 2.083
PDI of edge length (%)	5.46	5.33

As can be seen from Table 3, the polydispersity of Au Tetrahedra and Octahedra in terms of their edge length is quite low implying a good and successful synthesis method for their preparation.

Au monocrystalline spheres and AuBP@Ag 4 eq. (PRs):

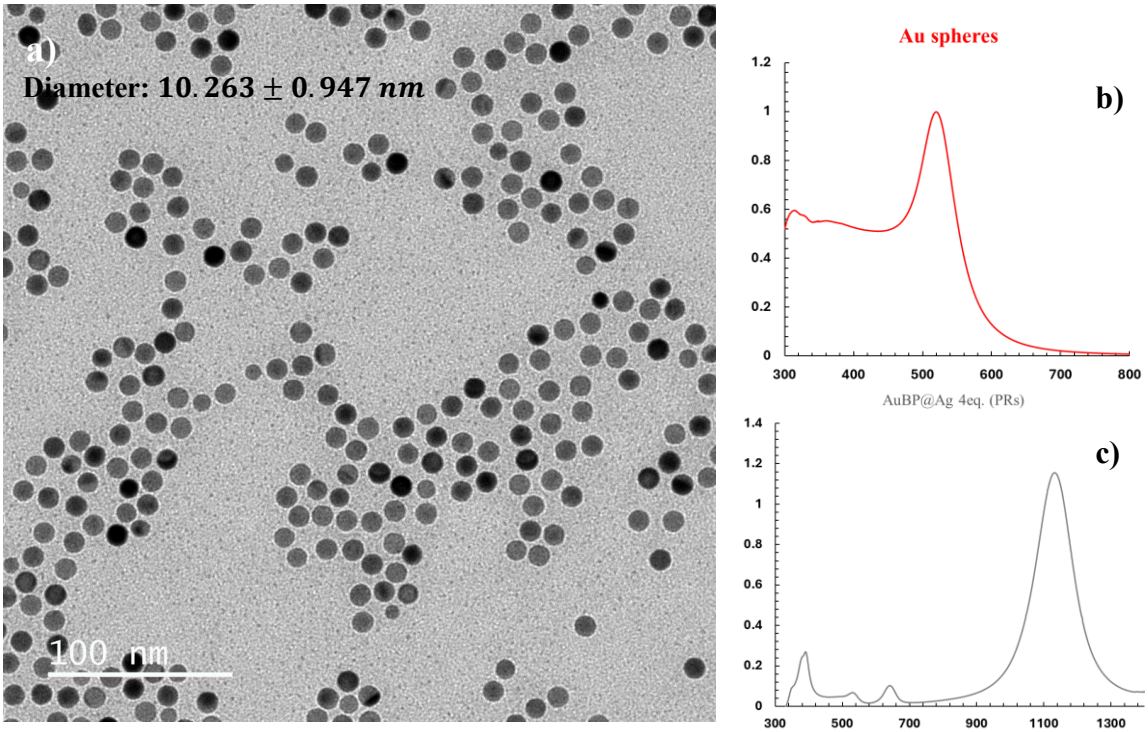


Fig. 15: TEM image a) and UV-Visible spectrum b) of Au monocrystalline spheres and c) UV-Visible spectrum of AuBP@Ag 4 eq. (PRs)

Fig. 15 represents the TEM image and UV-visible spectrum of Au monocrystalline spheres as well as the UV-visible spectrum of AuBP@Ag 4 eq. (PRs). The size of Au monocrystalline spheres is around 10 nm which was expected to be the case and in its UV-visible spectrum the major SPR band is around 521 nm which is very characteristic for Au spheres. UV-Visible spectrum of AuBP@Ag 4 eq. (PRs) contains many peaks that are hard to assign, but a very characteristic LSPR band around 1165 nm can be easily recognized. Moreover, the band around 391 nm is due to the high-order transverse modes.

3.3: Templated EISA of nanoparticles in prismatic confinement:

This section deals with the self-assembly of AuBP@Ag 4 eq. (PRs) and Au Tetrahedra in prismatic confinement. The self-assembly process is a result of a combination of templated effect and evaporation-induced self-assembly (EISA). Before discussing the results of template-assisted self-assembly of the above-mentioned NPs, the best combination of Au(0) and CTAC concentration was found to increase the reproducibility of self-assembly experiments and it will be discussed first.

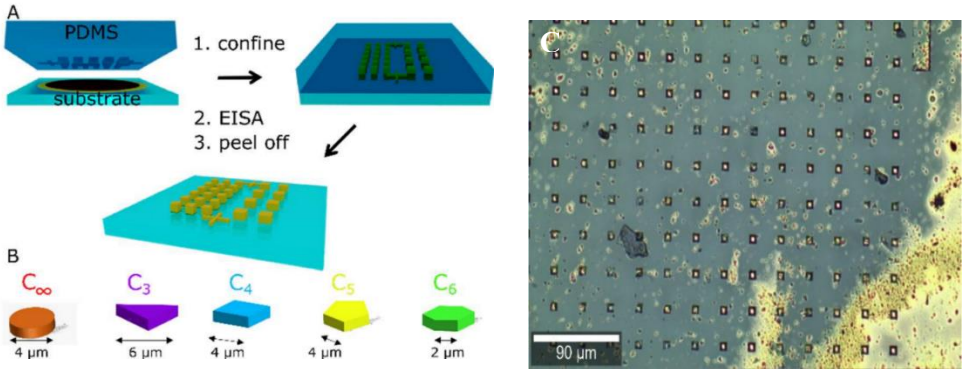


Fig. 16: Schematic of template-assisted EISA process[17] A), different shaped prisms used for template-assisted self-assembly of NPs[17] B), optical microscope image of filled square prisms C).

Fig. 16A schematically represents the template-assisted EISA process. During the self-assembly experiments 10 µL of concentrated suspensions of AuBP@Ag 4 eq. (PRs) and Au Tetrahedra were dropped on a PDMS mold and covered with glass or silicon wafer substrate. After 12-16 hours when the suspensions dried the substrate was carefully removed and depending on the type of prisms on the PDMS mold the respective SCs were formed on the substrate. Fig. 16C shows an optical microscope image of filled square prisms on a glass substrate.

Au(0)/CTAC concentration for templated EISA of Au NRs:

In this part of the project, the best combination of Au(0) and CTAC concentrations was determined for creating a protocol for future templated assisted self-assembly of metal NPs. For this reason, Si substrate was utilized which was cleaned beforehand. 50 mM, 250 mM, and 500 mM of Au(0), and 0.5 mM, 2.5 mM, and 10 mM of CTAC were utilized to find the best combination.

With low Au(0) concentration (50 mM) it was noticeable that the templates were not filled properly. No matter what was the concentration of CTAC the shapes were not well-defined and filled. Therefore, 50 mM of Au(0) concentration appeared to be a bad choice for templated self-assembly. The same arguments were true when the concentration of Au(0) was 250 mM, no matter the concentration of CTAC the shapes were not well-defined and filled.

Finally, Au(0) concentrations of 500 mM in 0.5 mM, 2.5 mM, and 10 mM of CTAC were investigated by optical microscope and the results can be seen below:

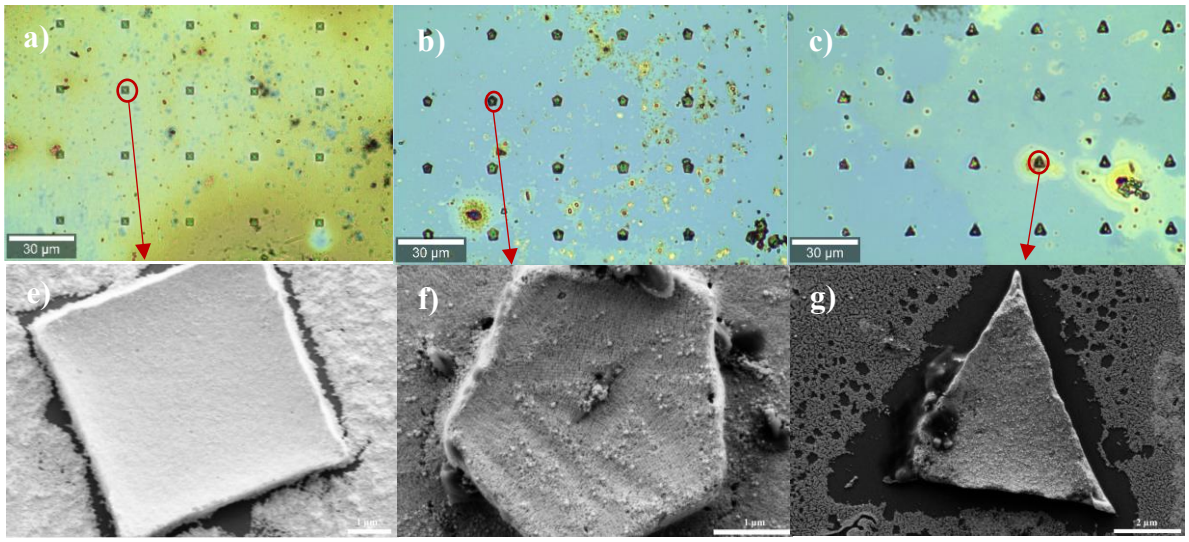


Fig. 17: Optical microscope images of: a) square prismatic templates (500 mM of Au(0)/0.5 mM of CTAC), b) pentagonal prismatic templates (500 mM of Au(0)/2.5 mM of CTAC), c) triangular prismatic templates (500 mM of Au(0)/10 mM of CTAC), and their corresponding SEM images e), f), g) respectively.

When the Au(0) concentration appeared to be 500 mM in all CTAC concentrations the templates were well-defined and well-filled. However, some interesting remarks can be made. In the case of 10 mM of CTAC concentration, CTAC seems to be on the top of the fillings at most shapes. In the case of 0.5 mM of CTAC, a lot of Au NPs seem to aggregate between the fillings. Whereas, for the case of 2.5 mM of CTAC the two aforementioned issues do not present. Moreover, the length and areas of the shapes were compared with each other to assess quantitively how well the templates were filled.

Table 3: Edge length and the area of the filled templates

Combination	Length±SD* (μm)	Area±SD (μm^2)
500 mM Au(0)/0.5 mM CTAC	3.724 ± 0.203	12.896 ± 0.917
500 mM Au(0)/2.5 mM CTAC	5.689 ± 0.331	21.998 ± 2.898
500 mM Au(0)/10 mM CTAC	5.338 ± 0.703	16.761 ± 3.101

*Standard deviation of the mean

As the values of edge length and area of the templates show the fillings are relatively similar sizes (low SD) for all concentrations of CTAC. Therefore, the optical microscope was useful for deducing Au(0) concentration whereas to select which CTAC concentration was the best SEM analysis was needed.

Based on SEM analysis when the concentration of CTAC was 0.5 mM (below its CMC value)[29], no local and long-range order was observed in the filled templates. The result is in agreement with

the literature[14,30] where they found that below the CMC concentration of cationic surfactants CTAC/CTAB monomer interaction with Au NPs promotes self-aggregation. It was clearly stated that critical concentration is necessary to form a bilayer on the Au NR surface[14], since the bilayer makes Au NPs to be charged positively and avoids aggregation. Moreover, the same publication stated that in the absence of the bilayer of Au NRs tend to aggregate due to strong van der Waals attraction forces. At CTAC concentration of 10 mM one can observe a lot of CTAC at the top of the filled shape, and the structure of Au NRs SC seems to be completely random. It is a well-known that phase separation of Au NRs and CTAC happens when the concentration of CTAC is too high.[14] Moreover, CTAC that is coated on the SC surface makes it very hard to characterize with SEM due to the excess electrostatic charge.[14] As can be observed for the 2.5 mM CTAC case the structure is well-ordered and there is no problem with CTAC coating on the SC surface meaning that it seems the best choice for templated assisted self-assembly. Based on the analysis Au(0) concentration of 500 mM and CTAC concentration of 2.5 mM was selected for future templated self-assembly experiments.

Template-assisted self-assembly of AuBP@Ag 4 eq. (PRs):

For the self-assembly experiments of AuBP@Ag 4 eq. (PRs) the total metal concentration (Au + Ag) was approximated to be 450 mM and the CTAC concentration was fixed to 2.5 mM (above its CMC). Below SEM results of template-assisted self-assembly of PRs in the case of square and triangular prisms can be seen:

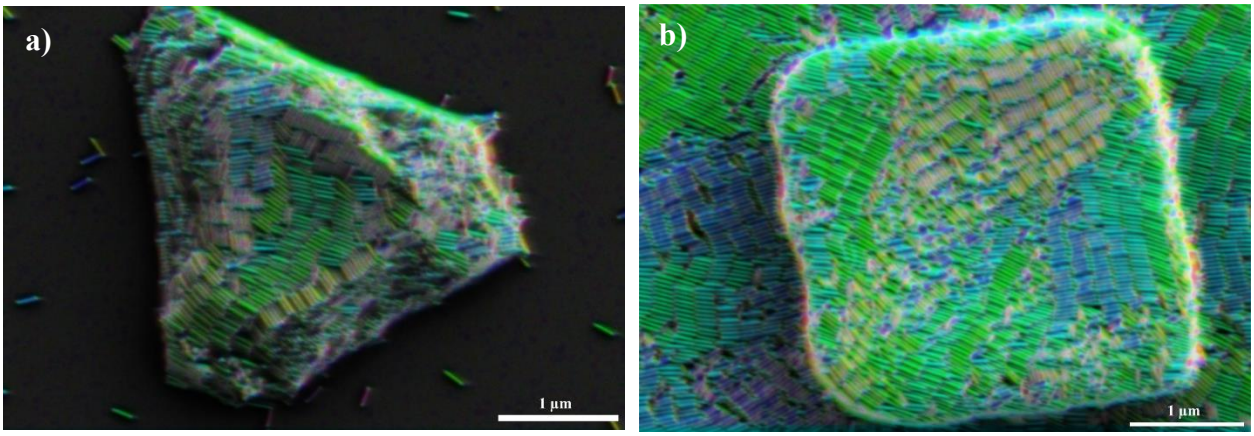


Fig. 18: Prismatic SCs formed by self-assembly of AuBP@Ag 4 eq. rods in (a) triangular and (b) square templates, different monodomains are color-encoded for better visibility of the different oriented monodomains.

Fig. 18 represents SEM images of template-assisted EISA of AuBP@Ag 4 eq. (PRs) in triangular (a) and square (b) prisms. It is noticeable that the long axis of the rods is mostly parallel to the substrate. Moreover, similar to Chaabani et al.[17] results the mold directs the growth of different monodomains for both prismatic geometries. For the case of a triangular prism, 3 ordered and differently oriented monodomains evenly spaced by $2\pi/3$ can be seen. In a square prism, there are 4 monodomains evenly spaced by $\pi/2$. Furthermore, since SEM can only give the information regarding one SC, it was imperative to perform 2D SAXS analysis to characterize hundreds of SCs[17] at the same time and present the average orientations of the SCs which can give more accurate information regarding the orientations of the formed assemblies.

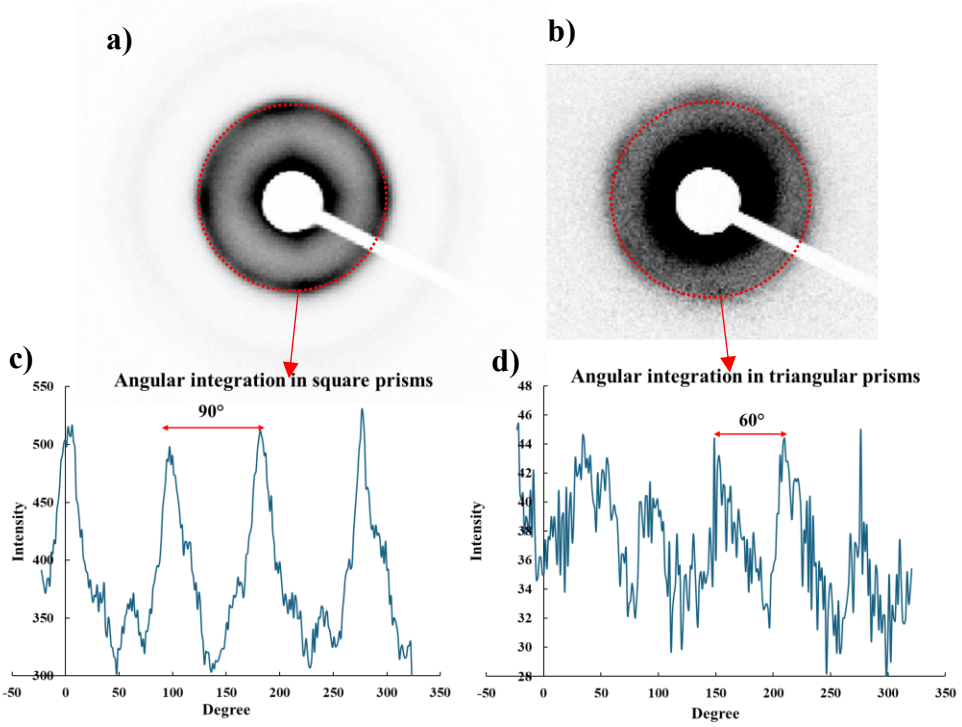


Fig. 19: 2D SAXS images a), b) and azimuthal integration analysis c), d) of square and triangular prismatic SCs.

From 2D SAXS images, one can conclude that on average the formed SCs were highly ordered (Bragg's spots indicate the order). From the 2D SAXS image of square prismatic SCs, 4 different Bragg's spots indicating the presence of 4 differently oriented monodomains were observed. Moreover, from azimuthal integration, it was noticeable that the spots were separated by 90º agreeing with SEM results. In the case of triangular prismatic SCs, 6 Bragg spots indicating the presence of 3 different monodomains were observed. Also, the Bragg's spots were separated by 60º which was expected to be the case. In general, 1 monodomain gives two equal Bragg's spots[17] separated by 180º. However, in the case of squares, two pairs of monodomains share the same orientations[17] which is the case for any prismatic templates which have even edges. Since, in triangular prismatic SCs, no two monodomains share the same orientations 6 Bragg's spots were observed. Furthermore, it is interesting to note that the prismatic SCs had rounded shapes instead of sharp points which can be explained by the presence of a meniscus formed due to the triple contact line at the air/water/substrate interface.[31] Finally, 2D to 1D data reduction was done for the case of square prismatic SCs by using Igor Pro software and the result can be seen below:

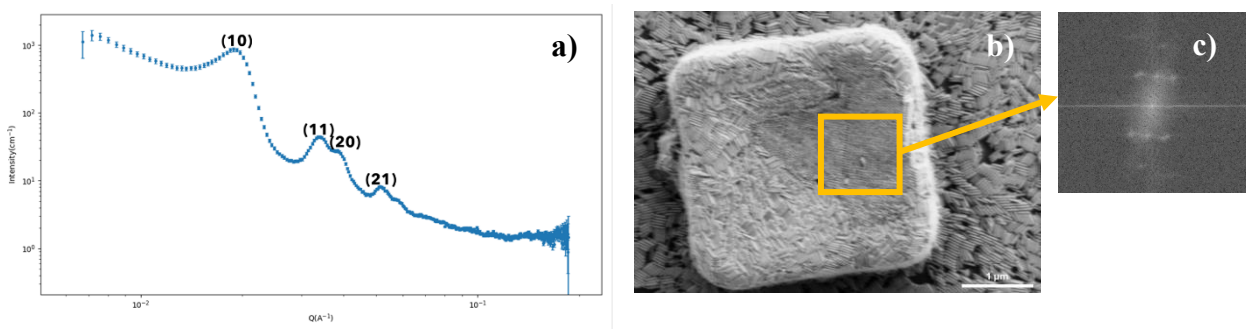


Fig. 20: From 2D to 1D data reduction for square template a), the square prismatic SC showing tip-to-tip assembly of PRs b) and FFT of the assembly c).

After 2D to 1D data reduction for the case of square prismatic SCs it was noticeable that the formed phase into which PRs self-assemble inside the square templates is 2D hexagonal. Since, $\boldsymbol{q_{10}}:\boldsymbol{q_{11}}:\boldsymbol{q_{20}}:\boldsymbol{q_{21}} = \mathbf{1}:\sqrt{\mathbf{3}}:\sqrt{\mathbf{4}}:\sqrt{\mathbf{7}}$ which is very characteristic of the 2D hexagonal phase. Moreover, the FFT pattern shown in Fig. 20c) is characteristic of either a 2D centered rectangular or 2D hexagonal phase.[17] However, one needs to use µSAXS experiments to correctly identify the formed structure within the prismatic SCs, since it provides characterization of a 3D structure of many individual SCs rather than providing the average result of many SCs at the same time.[17]

Template-assisted self-assembly of Au Tetrahedra:

For the templated EISA of Au Tetrahedra, the CTAC concentration was fixed to be 2.5 mM, while the Au(0) concentration was adjusted to be between 178 mM to 370 mM, since at 400 mM of Au(0) concentration it was noticed that Au Tetrahedra aggregate and do not fill the templates well.

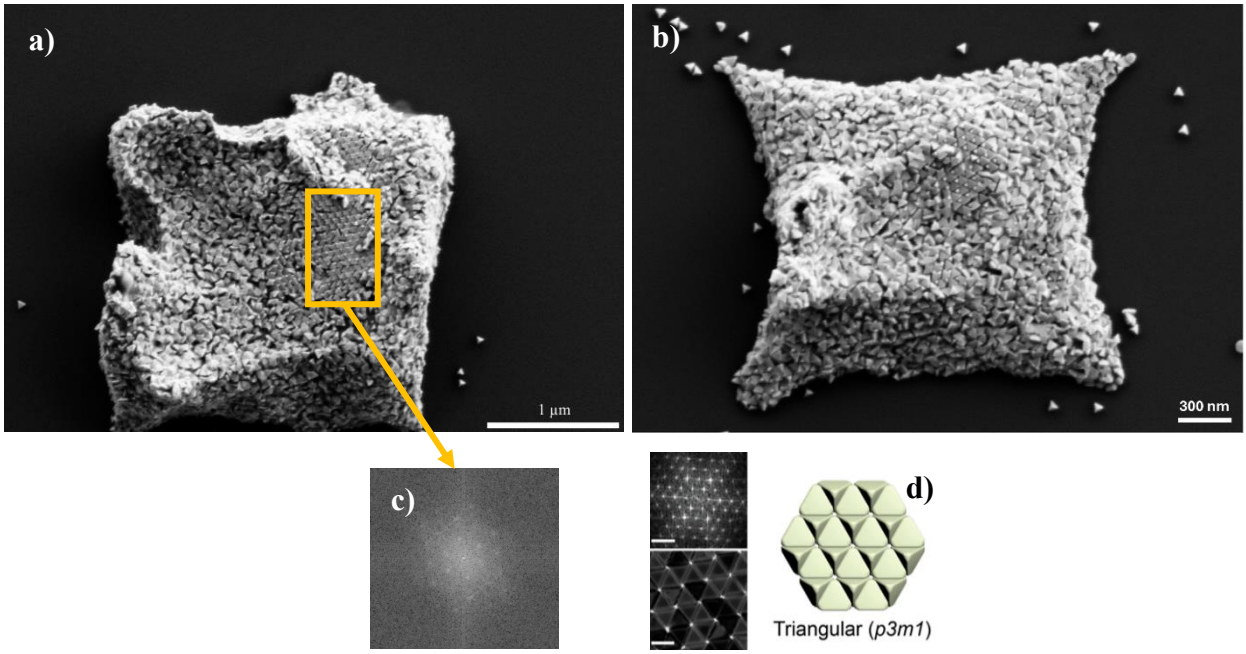
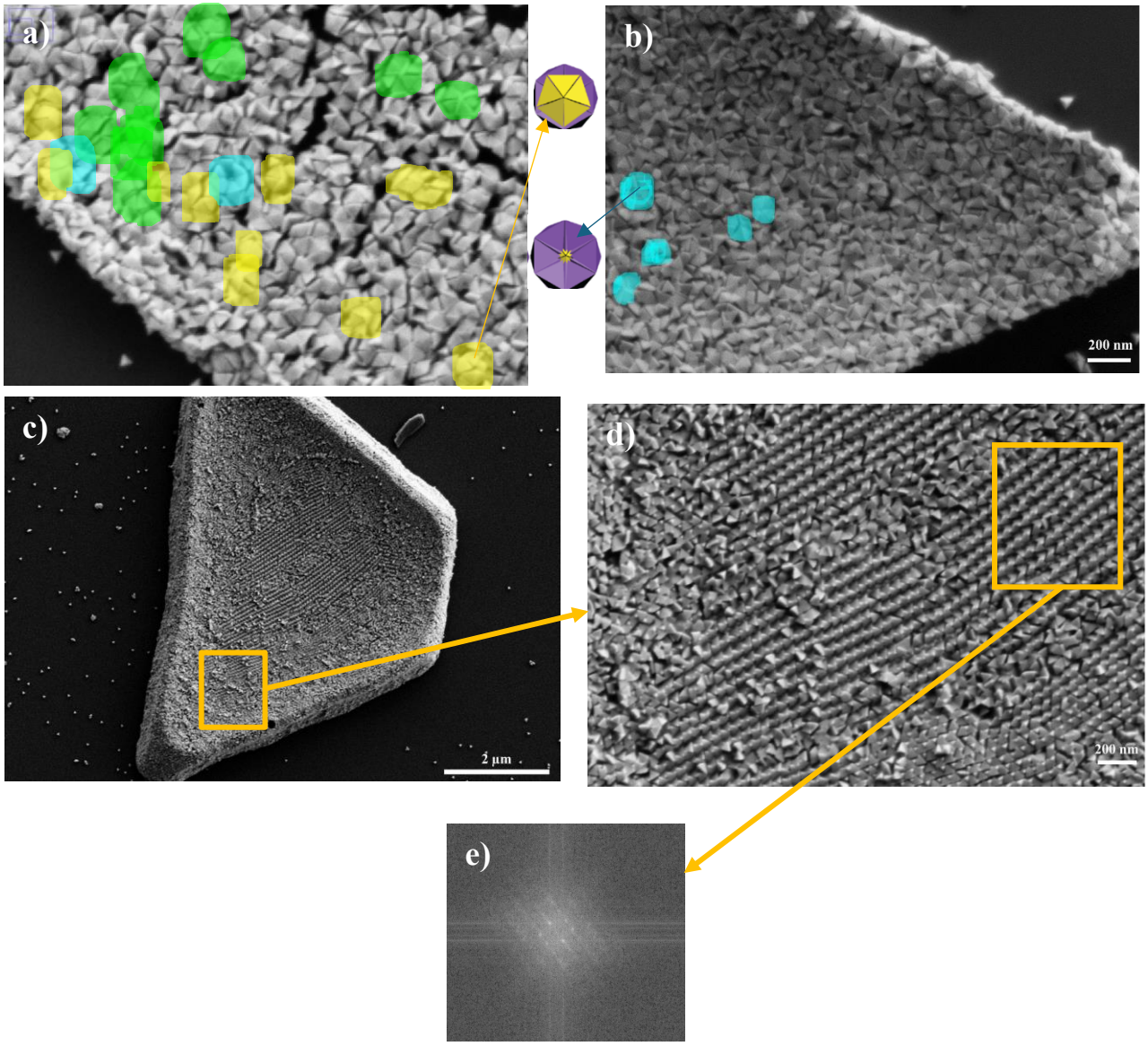


Fig. 21: SEM images of SCs of Au Tetrahedra in square prismatic templates a), b) the FFT of a) in the selected frame c), and typical FFT pattern for 2D triangular phase[15] d).

In the case of square prismatic SCs, Au Tetrahedra self-assemble into a very well-known hexagonal phase. Wang et al.[15] demonstrated that at an intermediate concentration of CTAC (0.1-2 mM), only hexagonal diamond and cubic diamond structures are formed, whereas at a high CTAC concentration $\geq$ 2 mM only hexagonal diamond structure is observed. Since the two mentioned structures are very hard to distinguish from the surface of the SCs, it is impossible to tell into which phase Au Tetrahedra self-assemble while forming the SCs. FFT of the surface of the SC shows the same pattern observed for the 2D triangular phase[15] which is a characteristic pattern for the hexagonal phase. It is interesting to note that the same structure is formed when the larger-sized SCs were assessed, and for some SCs the monolayer consisting of random assembly of Au Tetrahedra on the surface of the SCs was observed. For the triangular prismatic shapes the SEM results were slightly different and can be seen below:



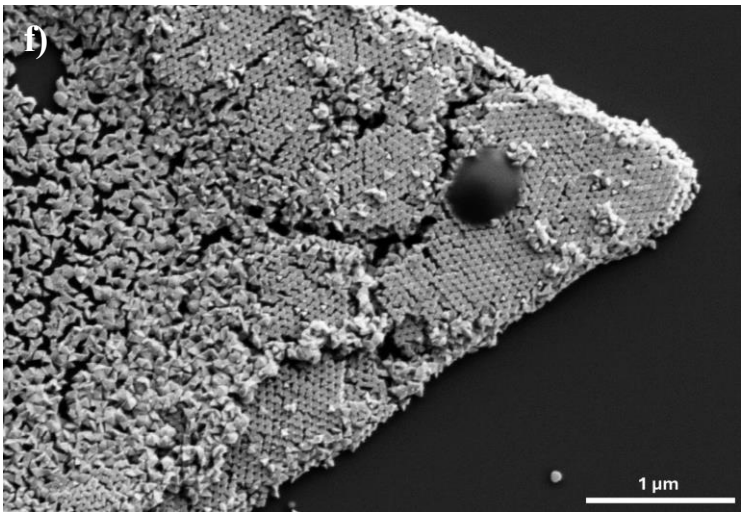


Fig. 22: SEM images of templated EISA of Au Tetrahedra in triangular prismatic templates showing some elements of dodecagonal quasicrystal[16] a), b), zig-zag-like structures c), d) and the presence of both hexagonal phase and elements of dodecagonal quasicrystal f), FFT of zig-zag-like structure e).

Templated EISA of Au Tetrahedra in triangular prismatic shapes was characterized by the formation of many phases and mixtures of different phases. For instance, from Fig. 22a), and b) it is apparent that in triangular prismatic shapes elements characteristic of dodecagonal quasicrystal were observed. In dodecagonal quasicrystal (QC) two pentagonal bipyramids (made from 5 Tetrahedra) sit above and below 12 Tetrahedra rings[16] and the pattern is repeated periodically within the depth of QC. Even though there is no such periodic pattern for the formed SCs in triangular prismatic shapes (Fig. 22a), and b)) the presence of the elements of QC is apparent. Moreover, in different shapes it was possible to see the mixture of the hexagonal phase and the elements of QC (Fig. 22f)). It was observed that elements of QC were mostly noticeable in monolayers, whereas the hexagonal phase was favored in 3D assemblies. Also, in some shapes it was noticed that Au Tetrahedra self-assemble into zig-zag-like structures (Fig. 22d)). Based on FFT it seems that the structure has a rectangular order, however, to exactly assess the structure one needs to perform µSAXS experiments. It is interesting to note that the same structures were observed when Au(0) concentration was between 178 mM to 370 mM. Therefore, one can argue that the structural diversity has little to do with Au(0) concentration. Other parameters decreasing CTAC concentration or solvent evaporation rate may result in structural diversities into which Au Tetrahedra self-assemble. However, it can be said with certainty that, unlike PRs, the formation of differently oriented monodomains growing from the edges of templates was not observed.

CONCLUSION AND PERSPECTIVES:

The templated EISA method made it possible to overcome limitations associated with the drop-casting method (due to the coffee-ring effect). The results suggested that the formed SCs were well-ordered and defined. Moreover, for the case of AuBP@Ag 4 eq. (PRs), the control of the orientations of the NPs within the SCs was achieved in prismatic confinement.

Similarly to Au monocrystalline NRs, prismatic confinement made it possible to successfully tune the number of oriented and ordered monodomains of AuBP@Ag 4 eq. (PRs) SCs. For triangular and square prismatic shapes, 3 and 4 monodomains similar to Au NRs were observed. Moreover, PRs self-assembled side-by-side manner similar to Au NRs, but as SAXS results indicated the structure into which PRs self-assemble is more likely to be 2D hexagonal rather than 2D centered rectangular[17] which appeared to be the case for Au NRs. The different nature of the tips and high AR of PRs made it possible to have a formation of a different structure than Au NRs which was expected to be the case.

The behavior of Au Tetrahedra under confinement was completely different than PRs which was expected to be the case. Au Tetrahedra possessed structural polymorphism within the same prismatic templates. In triangular prismatic shapes, various structures were observed which were less likely to be dependent on the concentration of Au(0). In square prismatic shapes, mostly triangular phase was seen in all sized SCs. One can conclude that triangular shapes have some effect on the formed structures which is not well understood yet. Moreover, unlike PRs no differently oriented monodomains were observed.

For future experiments, it is possible to try templated EISA of PRs in other prismatic shapes to see whether or not it is possible to tune the number of oriented and ordered monodomains. Moreover, it is possible to try different sizes and aspect ratios of PRs (2 eq. Ag, 8 eq. Ag) in prismatic confinement to assess the effect of AR on the structure and number of monodomains of the formed SCs. It is expected that due to the large AR of 8 eq. PRs the effect of confinement will be more pronounced. Furthermore, future experiments of templated EISA of Au Tetrahedra in different CTAC concentrations (below CMC) could be interesting because below CMC of CTAC the main force acting between Au Tetrahedra is attractive which could change the structure into which Au Tetrahedra self-assemble.

Finally, it can be said that the templated EISA process is not limited to only metal NPs and by the appropriate choice of ratio of curing agent and monomer[32], it is possible to make PDMS mold more resistant to organic solvents and self-assembly of perovskite NPs can be achieved.

REFERENCES:

(1) Xia, Y.; Campbell, D. J. Plasmons: Why Should We Care? *J. Chem. Educ.* **2007**, *84* (1), 91. https://doi.org/10.1021/ed084p91.

(2) Lu, X.; Rycenga, M.; Skrabalak, S. E.; Wiley, B.; Xia, Y. Chemical Synthesis of Novel Plasmonic Nanoparticles. *Annu. Rev. Phys. Chem.* **2009**, *60*, 167–192. https://doi.org/10.1146/annurev.physchem.040808.090434.

(3) Jana, J.; Ganguly, M.; Pal, T. Enlightening Surface Plasmon Resonance Effect of Metal Nanoparticles for Practical Spectroscopic Application. *RSC Adv* **2016**, *6* (89), 86174–86211. https://doi.org/10.1039/C6RA14173K.

(4) Sarfraz, N.; Khan, I. Plasmonic Gold Nanoparticles (AuNPs): Properties, Synthesis and Their Advanced Energy, Environmental and Biomedical Applications. *Chem. Asian J.* **2021**, *16* (7), 720–742. https://doi.org/10.1002/asia.202001202.

(5) Rechberger, W.; Hohenau, A.; Leitner, A.; Krenn, J. R.; Lamprecht, B.; Aussenegg, F. R. Optical Properties of Two Interacting Gold Nanoparticles. *Opt. Commun.* **2003**, *220* (1), 137–141. https://doi.org/10.1016/S0030-4018(03)01357-9.

(6) García-Lojo, D.; Núñez-Sánchez, S.; Gómez-Graña, S.; Grzelczak, M.; Pastoriza-Santos, I.; Pérez-Juste, J.; Liz-Marzán, L. M. Plasmonic Supercrystals. *Acc. Chem. Res.* **2019**, *52* (7), 1855–1864. https://doi.org/10.1021/acs.accounts.9b00213.

(7) ABERASTURI, D. J. D.; HAMON, C.; LIZ-MARZ?N, L. M. Chemical Synthesis of Plasmonic Nanoparticles. In *World Scientific Handbook of Metamaterials and Plasmonics*; World Scientific Series in Nanoscience and Nanotechnology; World Scientific, 2017; pp 439–473. https://doi.org/10.1142/9789813228726_0012.

(8) Murphy, C. J.; Thompson, L. B.; Alkilany, A. M.; Sisco, P. N.; Boulos, S. P.; Sivapalan, S. T.; Yang, J. A.; Chernak, D. J.; Huang, J. The Many Faces of Gold Nanorods. *J. Phys. Chem. Lett.* **2010**, *1* (19), 2867–2875. https://doi.org/10.1021/jz100992x.

(9) Scarabelli, L.; Sánchez-Iglesias, A.; Pérez-Juste, J.; Liz-Marzán, L. M. A "Tips and Tricks" Practical Guide to the Synthesis of Gold Nanorods. *J. Phys. Chem. Lett.* **2015**, *6* (21), 4270–4279. https://doi.org/10.1021/acs.jpclett.5b02123.

(10) Xia, Y.; Gilroy, K. D.; Peng, H.-C.; Xia, X. Seed-Mediated Growth of Colloidal Metal Nanocrystals. *Angew. Chem. Int. Ed.* **2017**, *56* (1), 60–95. https://doi.org/10.1002/anie.201604731.

(11) Han, W.; Lin, Z. Learning from "Coffee Rings": Ordered Structures Enabled by Controlled Evaporative Self-Assembly. *Angew. Chem. Int. Ed Engl.* **2012**, *51* (7), 1534–1546. https://doi.org/10.1002/anie.201104454.

(12) Deng, K.; Luo, Z.; Tan, L.; Quan, Z. Self-Assembly of Anisotropic Nanoparticles into Functional Superstructures. *Chem Soc Rev* **2020**, *49* (16), 6002–6038. https://doi.org/10.1039/D0CS00541J.

(13) Reichhelm, A.; Haubold, D.; Eychmüller, A. Ligand Versatility in Supercrystal Formation. *Adv. Funct. Mater.* **2017**, *27* (39), 1700361. https://doi.org/10.1002/adfm.201700361.

(14) Ming, T.; Kou, X.; Chen, H.; Wang, T.; Tam, H.-L.; Cheah, K.-W.; Chen, J.-Y.; Wang, J. Ordered Gold Nanostructure Assemblies Formed By Droplet Evaporation. *Angew. Chem. Int. Ed.* **2008**, *47* (50), 9685–9690. https://doi.org/10.1002/anie.200803642.

(15) Wang, Y.; Chen, J.; Zhong, Y.; Jeong, S.; Li, R.; Ye, X. Structural Diversity in Dimension-Controlled Assemblies of Tetrahedral Gold Nanocrystals. *J. Am. Chem. Soc.* **2022**, *144* (30), 13538–13546. https://doi.org/10.1021/jacs.2c03196.

(16) Wang, Y.; Chen, J.; Li, R.; Götz, A.; Drobek, D.; Przybilla, T.; Hübner, S.; Pelz, P.; Yang, L.; Apeleo Zubiri, B.; Spiecker, E.; Engel, M.; Ye, X. Controlled Self-Assembly of Gold Nanotetrahedra into Quasicrystals and Complex Periodic Supracrystals. *J. Am. Chem. Soc.* **2023**, *145* (32), 17902–17911. https://doi.org/10.1021/jacs.3c05299.

(17) Chaâbani, W.; Lyu, J.; Marcone, J.; Goldmann, C.; ten Veen, E. J. M.; Dumesnil, C.; Bizien, T.; Smallenburg, F.; Impéror-Clerc, M.; Constantin, D.; Hamon, C. Prismatic Confinement Induces

Tunable Orientation in Plasmonic Supercrystals. *ACS Nano* **2024**, *18* (13), 9566–9575. https://doi.org/10.1021/acsnano.3c12799.
(18) Wang, D.; Hermes, M.; Kotni, R.; Wu, Y.; Tasios, N.; Liu, Y.; de Nijs, B.; van der Wee, E. B.; Murray, C. B.; Dijkstra, M.; van Blaaderen, A. Interplay between Spherical Confinement and Particle Shape on the Self-Assembly of Rounded Cubes. *Nat. Commun.* **2018**, *9* (1), 2228. https://doi.org/10.1038/s41467-018-04644-4.
(19) Wan, S.; Xi, X.; Zhang, H.; Ning, J.; Zheng, Z.; Zhang, Z.; Long, Y.; Deng, Y.; Fan, P.; Yang, D.; Li, T.; Dong, A. Shape-Mediated Oriented Assembly of Concave Nanoparticles under Cylindrical Confinement. *ACS Nano* **2022**, *16* (12), 21315–21323. https://doi.org/10.1021/acsnano.2c09479.
(20) Cheng, Z.; Jones, M. R. Assembly of Planar Chiral Superlattices from Achiral Building Blocks. *Nat. Commun.* **2022**, *13* (1), 4207. https://doi.org/10.1038/s41467-022-31868-2.
(21) Qin, D.; Xia, Y.; Whitesides, G. M. Soft Lithography for Micro- and Nanoscale Patterning. *Nat. Protoc.* **2010**, *5* (3), 491–502. https://doi.org/10.1038/nprot.2009.234.
(22) Jeffries, C. M.; Ilavsky, J.; Martel, A.; Hinrichs, S.; Meyer, A.; Pedersen, J. S.; Sokolova, A. V.; Svergun, D. I. Small-Angle X-Ray and Neutron Scattering. *Nat. Rev. Methods Primer* **2021**, *1* (1), 70. https://doi.org/10.1038/s43586-021-00064-9.
(23) Stieger, M.; Richtering, W.; Pedersen, J. S.; Lindner, P. Small-Angle Neutron Scattering Study of Structural Changes in Temperature Sensitive Microgel Colloids. *J. Chem. Phys.* **2004**, *120* (13), 6197–6206. https://doi.org/10.1063/1.1665752.
(24) Sánchez-Iglesias, A.; Winckelmans, N.; Altantzis, T.; Bals, S.; Grzelczak, M.; Liz-Marzán, L. M. High-Yield Seeded Growth of Monodisperse Pentatwinned Gold Nanoparticles through Thermally Induced Seed Twinning. *J. Am. Chem. Soc.* **2017**, *139* (1), 107–110. https://doi.org/10.1021/jacs.6b12143.
(25) Zheng, Y.; Liu, W.; Lv, T.; Luo, M.; Hu, H.; Lu, P.; Choi, S.-I.; Zhang, C.; Tao, J.; Zhu, Y.; Li, Z.-Y.; Xia, Y. Seed-Mediated Synthesis of Gold Tetrahedra in High Purity and with Tunable, Well-Controlled Sizes. *Chem. – Asian J.* **2014**, *9* (9), 2635–2640. https://doi.org/10.1002/asia.201402499.
(26) Scarabelli, L.; Grzelczak, M.; Liz-Marzán, L. M. Tuning Gold Nanorod Synthesis through Prereduction with Salicylic Acid. *Chem. Mater.* **2013**, *25* (21), 4232–4238. https://doi.org/10.1021/cm402177b.
(27) Gómez-Graña, S.; Fernández-López, C.; Polavarapu, L.; Salmon, J.-B.; Leng, J.; Pastoriza-Santos, I.; Pérez-Juste, J. Gold Nanooctahedra with Tunable Size and Microfluidic-Induced 3D Assembly for Highly Uniform SERS-Active Supercrystals. *Chem. Mater.* **2015**, *27* (24), 8310–8317. https://doi.org/10.1021/acs.chemmater.5b03620.
(28) Navarro, J. R. G.; Manchon, D.; Lerouge, F.; Blanchard, N. P.; Marotte, S.; Leverrier, Y.; Marvel, J.; Chaput, F.; Micouin, G.; Gabudean, A.-M.; Mosset, A.; Cottancin, E.; Baldeck, P. L.; Kamada, K.; Parola, S. Synthesis of PEGylated Gold Nanostars and Bipyramids for Intracellular Uptake. *Nanotechnology* **2012**, *23* (46), 465602. https://doi.org/10.1088/0957-4484/23/46/465602.
(29) Sepulveda, L.; Cortes, J. Ionization Degrees and Critical Micelle Concentrations of Hexadecyltrimethylammonium and Tetradecyltrimethylammonium Micelles with Different Counterions. *J. Phys. Chem.* **1985**, *89* (24), 5322–5324. https://doi.org/10.1021/j100270a040.
(30) Kazakova, J.; García-Povea, A.; Fernández-Palacios, M.; Villar-Navarro, M.; Carnerero, J. M.; Jimenez-Ruiz, A.; Prado-Gotor, R. A Colorimetric Study of the Interaction of Cationic and Anionic Surfactants with Anionic Gold Nanoparticles. *Colloid Polym. Sci.* **2017**, *295* (11), 2141–2149. https://doi.org/10.1007/s00396-017-4186-6.
(31) Hamon, C.; Sanz-Ortiz, M. N.; Modin, E.; Hill, E. H.; Scarabelli, L.; Chuvilin, A.; Liz-Marzán, L. M. Hierarchical Organization and Molecular Diffusion in Gold Nanorod/Silica Supercrystal Nanocomposites. *Nanoscale* **2016**, *8* (15), 7914–7922. https://doi.org/10.1039/C6NR00712K.
(32) Aftenieva, O.; Brunner, J.; Adnan, M.; Sarkar, S.; Fery, A.; Vaynzof, Y.; König, T. A. F. Directional Amplified Photoluminescence through Large-Area Perovskite-Based Metasurfaces. *ACS Nano* **2023**, *17* (3), 2399–2410. https://doi.org/10.1021/acsnano.2c09482.